

# Catalytic Oxidation of Methane to Oxygenated Products: Recent Advancements and Prospects for Electrocatalytic and Photocatalytic Conversion at Low Temperatures

Md. Selim Arif Sher Shah, Cheoulwoo Oh, Hyesung Park, Yun Jeong Hwang, Ming Ma,\* and Jong Hyeok Park\*

Methane is an important fossil fuel and widely available on the earth's crust. It is a greenhouse gas that has more severe warming effect than CO<sub>2</sub>. Unfortunately, the emission of methane into the atmosphere has long been ignored and considered as a trivial matter. Therefore, emphatic effort must be put into decreasing the concentration of methane in the atmosphere of the earth. At the same time, the conversion of less valuable methane into value-added chemicals is of significant importance in the chemical and pharmaceutical industries. Although, the transformation of methane to valuable chemicals and fuels is considered the "holy grail," the low intrinsic reactivity of its C–H bonds is still a major challenge. This review discusses the advancements in the electrocatalytic and photocatalytic oxidation of methane at low temperatures with products containing oxygen atom(s). Additionally, the future research direction is noted that may be adopted for methane oxidation via electrocatalysis and photocatalysis at low temperatures.

## 1. Introduction

Methane (CH<sub>4</sub>), as the simplest saturated hydrocarbon with the lowest C/H ratio,<sup>[1]</sup> owns a high calorific value.<sup>[2–4]</sup> The combustion of CH<sub>4</sub> could release more energy per molecule of produced CO<sub>2</sub> compared to oil (approximately CH<sub>2</sub>) or coal (approximately CH).<sup>[5,6]</sup> CH<sub>4</sub> has been abundantly found on the earth, due to its high stability.<sup>[7]</sup> Natural gas, one of the main existing form for CH<sub>4</sub> (about 70–90% by volume), is plentiful in the crust around the world, constituting ≈21% of total principal energy sources on the earth. For instance, CH<sub>4</sub> molecules could be held with water through hydrogen bonding in the form of methane hydrates (combustible ice), existing in the continental slopes of oceans, marine sediments, cold climate regions, and subsurface deposits.<sup>[8,9]</sup> The amount of methane hydrates has been estimated about (3000–20 000) × 10<sup>12</sup> m<sup>3</sup>,<sup>[10,11]</sup> with energy calculated to be more than double of that from all other fossil fuels.<sup>[12]</sup> Natural gas has been exploited from shale gas recently, the amount of which is estimated to be more than 7299 trillion cubic feet.<sup>[13–17]</sup> Methane also could be naturally generated from biosystems as marsh gas through the anaerobic digestion of crops, wastes and residues.<sup>[18,19]</sup> Human activities, such as coal mining, natural gas or petroleum drilling and breakdown of garbage in landfills, significantly contribute to the release of CH<sub>4</sub>. The main existence form of CH<sub>4</sub> could be classified in **Figure 1**.


According to the abundant reserves, CH<sub>4</sub> fuels possess superior economic efficiency with a high energy density (>1000 kWh m<sup>-3</sup>).<sup>[20]</sup> CH<sub>4</sub> could be burned directly with oxygen to obtain high amount of heat energy ( $\Delta H_{298K}^0 = -802 \text{ kJ mol}^{-1}$ ),<sup>[21]</sup> or catalytically oxidized to generate electrical energy in fuel cells.<sup>[22,23]</sup> Thus, as a cleaner energy compared to other conventional fuels,<sup>[24,25,26–28]</sup> CH<sub>4</sub> alone has the potential to compensate for the depletion of fossil fuel. However, it is a powerful greenhouse gas that exhibits a global radiative forcing of 0.61 W m<sup>-2</sup>, which amounts to ≈20% of all the greenhouse gases in 2011.<sup>[29,30]</sup> As the CH<sub>4</sub> sources are mainly stored in depopulated areas, the exploitation and transportation of them to industrial areas are not economically viable.<sup>[31,32]</sup> In the atmosphere, the concentration of CH<sub>4</sub> rose from 722 parts per billion (ppb) in the preindustrial era to 1867 ppb in 2018 with an over 2.5-fold increase.<sup>[6]</sup> The CH<sub>4</sub>

Dr. M. S. A. Sher Shah, C. Oh, Dr. Y. J. Hwang, Prof. J. H. Park  
Department of Chemical and Biomolecular Engineering  
Yonsei University  
50 Yonsei-ro, Seodaemun-gu, Seoul 03722, Republic of Korea  
E-mail: lutts@yonsei.ac.kr

Prof. H. Park  
Department of Energy Engineering  
School of Energy and Chemical Engineering  
Low Dimensional Carbon Materials Center  
Perovtronics Research Center  
Ulsan National Institute of Science and Technology (UNIST)  
Ulsan 44919, Republic of Korea

Dr. Y. J. Hwang, Prof. J. H. Park  
Clean Energy Research Center  
Korea Institute of Science and Technology (KIST)  
Seoul 02792, Republic of Korea

Prof. M. Ma  
Shenzhen Institutes of Advanced Technology  
Chinese Academy of Sciences  
Shenzhen, Guangdong 518055, China  
E-mail: ming.ma@siat.ac.cn

 The ORCID identification number(s) for the author(s) of this article can be found under <https://doi.org/10.1002/advs.202001946>

© 2020 The Authors. Published by Wiley-VCH GmbH. This is an open access article under the terms of the Creative Commons Attribution License, which permits use, distribution and reproduction in any medium, provided the original work is properly cited.

DOI: 10.1002/advs.202001946

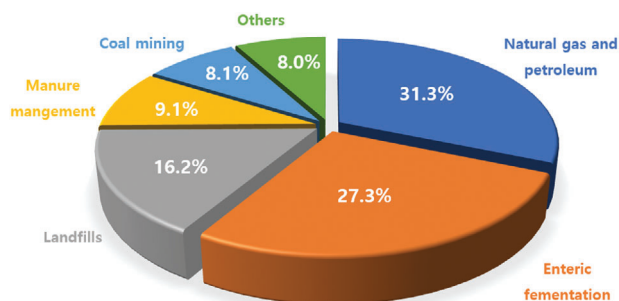


**Figure 1.** Distribution proportion of different CH<sub>4</sub> sources.

emission affects the earth's climate and global energy balance. Therefore, diminishing the leakage of CH<sub>4</sub> is essential to decreasing global warming, pollution and climate change. Conversion of CH<sub>4</sub> to value added chemicals is the most significant way to control its emission during the human activities. In this case, especially if converted at low temperatures, industrially important chemicals can be produced simultaneously. Unfortunately, most of the conversion processes are kinetically sluggish at low temperature due to the intrinsic inertness of CH<sub>4</sub>,<sup>[21,33,34]</sup> requiring relatively high temperature (and pressure) to carry out these reactions.<sup>[35]</sup>

Up to now, numerous works have been done upon the conversion of CH<sub>4</sub>, with diversified review reports published. Most of the review works on CH<sub>4</sub> conversion have involved several interests, such as partial oxidation over transition metal-based catalysts,<sup>[36–39]</sup> oxidation of CH<sub>4</sub> by heterogeneous catalysts,<sup>[40,41]</sup> metal organic framework-based catalysts for CH<sub>4</sub> oxidation,<sup>[41]</sup> complete oxidation of CH<sub>4</sub>,<sup>[7,42–44]</sup> and electrocatalytic CH<sub>4</sub> oxidation at high temperatures.<sup>[36,45]</sup> However, the theme of CH<sub>4</sub> partial oxidation at low temperature is rare.<sup>[46]</sup> Moreover, the fundamental chemical properties and the inertness origin for CH<sub>4</sub> were neglected in those reviews. This review is devoted to the CH<sub>4</sub> oxidation by electrocatalytic and photocatalytic processes at low temperatures, especially at room temperature.

In this review, we have discussed the chemistry behind the inertness of CH<sub>4</sub>, the significance for CH<sub>4</sub> oxidation and challenges therein, and various processes for C–H activation with emphasis on electrocatalytic and photocatalytic routes, especially at room/low temperatures. The scope of this review is focused on the CH<sub>4</sub> oxidation processes, involving with the cleavage of the C–H bonds and subsequent functionalization of the carbon atoms. For highlighting the particularity and professionalism of this review, we aim at the well-defined systems leading to the production of oxygenates from CH<sub>4</sub> oxidation, excluding higher alkanes, halides or any other compounds without oxygen. At the end, we will outline the future research directions that researchers would like to adopt for efficient CH<sub>4</sub> oxidation, which would be timely contribution to the energy conversion fields.

## 2. Intrinsic Motivation for CH<sub>4</sub> Oxidation

### 2.1. The “Inert” Chemistry of CH<sub>4</sub>

At normal pressure and temperature, CH<sub>4</sub> expresses colorless and odorless gas. It possesses tetrahedral molecular structure

(Figure 2a) consisting of four equivalent C–H bonds, according to the sp<sup>3</sup> hybridization of the carbon atom (point group T<sub>d</sub>, C–H bond length of 1.087 Å and H–C–H bond angle of 109.5°).<sup>[40]</sup> Due to the directional orientation, sp<sup>3</sup> bonding orbitals are less well-adapted to the formation of new bonds in the transition state, resulting in a barrier restricting the chemical reactions. The CH<sub>4</sub> molecule has immense stability and symmetry with a small polarizability (2.84 × 10<sup>−40</sup> C<sup>2</sup> m<sup>2</sup> J<sup>−1</sup>),<sup>[47]</sup> due to the small electronegativity difference between carbon (2.55) and hydrogen (2.2).<sup>[48]</sup> As a result, a comparatively high local electric field is needed to induce polarization and to allow electrophilic or nucleophilic attack of CH<sub>4</sub> for initiating chemical reactions. Notably, the carbon atom in CH<sub>4</sub> is slightly negatively charged (δ<sub>C</sub> = −0.185), while the hydrogen atoms get a slightly positive charge (δ<sub>H</sub> = +0.046).<sup>[49]</sup> The CH<sub>4</sub> molecule contains four bonding molecular orbitals (Figure 2b) that are formed by the overlap of the four valence orbitals of the central carbon atom and one valence orbital from each of the four hydrogen atoms.

CH<sub>4</sub> has triply degenerate molecular orbitals produced as a result of the overlap of two 2p carbon orbitals and three 1s orbitals of the hydrogen atoms. In the ground electronic state (X<sup>1</sup>A<sub>1</sub>), all electrons occupy bonding molecular orbitals with an electronic configuration of (1a<sub>1</sub>)<sup>2</sup>(1t<sub>2</sub>)<sup>6</sup>(2a<sub>1</sub>)<sup>0</sup>.<sup>[50]</sup> The absence of electrons in the antibonding molecular orbitals (σ\*) guarantees the sturdy stability of CH<sub>4</sub> molecule.<sup>[51]</sup> Moreover, the absence of low-lying empty orbitals (σ molecular orbitals) and high-energy filled orbitals (σ\* molecular orbitals) (Figure 2b) make the participation of CH<sub>4</sub> in any chemical reaction tough.<sup>[4,52]</sup> The highest occupied molecular orbital (HOMO) in CH<sub>4</sub> has low energy and the lowest unoccupied molecular orbital (LUMO) has high energy. As a result, it is challenging to remove electrons from the HOMO or to add them to the LUMO of CH<sub>4</sub>.<sup>[47,53]</sup> The absence of lone electron pairs that can be relatively easily attacked is another reason for the inertness of methane. Furthermore, CH<sub>4</sub> is highly resilient to nucleophilic attack because electron donation to the high-energy σ\* molecular orbital is energetically unfavorable and sterically hindered.

Compared to the other alkane, CH<sub>4</sub> contains four unusually strong localized C–H bonds (the bond energy of H–CH<sub>3</sub> was calculated to be 439.3 kJ mol<sup>−1</sup> under standard conditions).<sup>[33,54,55]</sup> Therefore, C–H bond scissions for CH<sub>4</sub> (both homolytic and heterolytic) are not feasible. In a contrast, methyl cations (CH<sub>3</sub><sup>+</sup>) are the least stable carbocations, which make methane the least reactive alkane for the abstraction of hydride ions. Highly negative electron affinity (≈−1.9 eV) indicates CH<sub>4</sub><sup>−</sup> anion is less stable than CH<sub>4</sub> itself.<sup>[56]</sup> Additionally, CH<sub>4</sub> possesses critically unreactive C–H bonds for any electron transfer reaction due to its high ionization energy (≈12.6 eV).<sup>[57]</sup> The low proton affinity (543.9 kJ mol<sup>−1</sup>)<sup>[58]</sup> and weak acidity (pK<sub>a</sub> ≈ 48)<sup>[59]</sup> restrict its activation by any acid or base. Nevertheless, removal of the electrons from the σ bonds in CH<sub>4</sub> by strong electrophiles, although challenging, is somewhat facile. Homolytic cleavage of the C–H bonds, followed by the formation of hydrogen radical and methyl radical, is the most facile way for CH<sub>4</sub> oxidation.<sup>[60]</sup> However, CH<sub>4</sub> should be a choice for reactions involving sufficiently hindered reagents due to its small size.

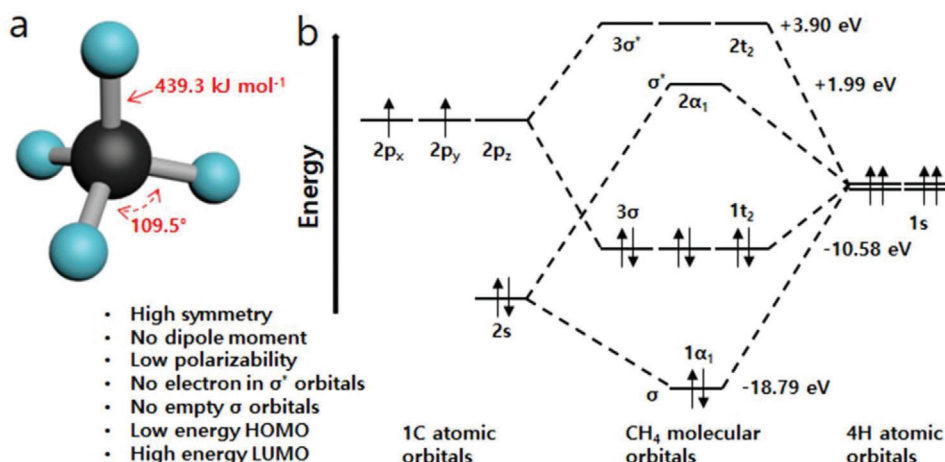


**Figure 2.** a) CH<sub>4</sub> tetrahedral structure. b) Molecular orbital diagram with the corresponding energies, source: [https://www.science.oregonstate.edu/~gablek/CH334/Chapter1/methane\\_MOs.htm](https://www.science.oregonstate.edu/~gablek/CH334/Chapter1/methane_MOs.htm).

## 2.2. Challenges and Significances of CH<sub>4</sub> Oxidation

Conversion of CH<sub>4</sub> to its derivatives at low temperatures through direct pathways is kinetically challenging.<sup>[61]</sup> For cleaving the C–H bonds and thereby oxidizing the molecule to any oxygenated products (except CO<sub>2</sub>), a large amount of energy usually should be provided. Often, this amount of energy is supplied from thermal energy by increasing the reaction temperature. In reality, to achieve CH<sub>4</sub> oxidation, the reaction would always be operated at fairly high temperatures (>≈700 °C), which generally leads to reactions driven by a free radical mechanism with intrinsic low selectivity.<sup>[40]</sup> High temperature conditions, always along with high pressures, indicate high costs for industrial applications, in addition to safety issues. The low solubility of gaseous CH<sub>4</sub> (compared to the good solubility of the related oxidation products) imparts another challenge for its oxidation.<sup>[46]</sup> Thus, the concentration of the oxidation products would be much higher than that of CH<sub>4</sub> in any reaction mixture, accompanying with severe side reactions, which could generate serious selectivity issues for the products formation.

Other issues, such as the stability and durability of catalysts and the formation of CO<sub>2</sub>, should also be considered for CH<sub>4</sub> oxidation at high temperatures and pressures. For highly efficient CH<sub>4</sub> oxidation, noble metals (such as Pt, Ir, Ru, Rh, and Pd) are frequently employed as catalysts, which are expensive and rare. Thus, the valuable CH<sub>4</sub> oxidation suffers highly energy demanding, expensive processes that are challenging for industries. In the meantime, the superior activity of CH<sub>4</sub> oxidation products and other intermediates compared to CH<sub>4</sub> itself (e.g., C–H bond dissociation energy in CH<sub>3</sub>OH is 0.4 eV less than that in methane) would cause excessive oxidation of CH<sub>4</sub>.<sup>[62,63]</sup> Naturally, stopping further oxidation is quite difficult even methanol has been formed locally by a catalyst at low temperatures,<sup>[64]</sup> as depicted in **Figure 3**. Therefore, kinetic protection and selective separation of the products are necessary to obtain the desired products, making the oxidation process more complex. These challenges in CH<sub>4</sub> oxidation result in a small number of industrial applications.

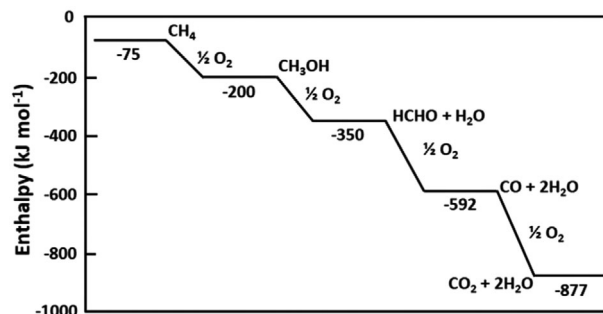


**Figure 3.** Changes in enthalpy at 298 K for successive oxidation of CH<sub>4</sub>. Reproduced with permission.<sup>[62]</sup> Copyright 1991, Elsevier.

On the other hand, CH<sub>4</sub> oxidation is important due to several reasons such as decreasing the global warming. CH<sub>4</sub> can also be used as raw material to produce useful chemicals,<sup>[65–68]</sup> especially as hydrogen (energy density of 270 kWh m<sup>-3</sup>),<sup>[20]</sup> which is considered as the cleanest and greenest energy source in addition to being one of the world's most important chemicals.<sup>[69–71]</sup> Notably, ≈50% of the world's demand for hydrogen (almost 55 × 10<sup>6</sup> ton per year) derives from natural gas.<sup>[72,73]</sup> CH<sub>4</sub> is a vital source of valuable chemicals, such as methanol and CO. Moreover, CH<sub>4</sub> could not be easily liquefied (critical temperature –82.3 °C) at practically accessible low temperatures,<sup>[6]</sup> causing transportation problems in remote areas. The main challenges and significance of CH<sub>4</sub> oxidation has been summarized in **Figure 4**.

## 3. Processes for CH<sub>4</sub> Oxidation

Partial oxidation of CH<sub>4</sub> leads to the formation of value-added chemicals that can be used in the chemical and energy sectors and the pharmaceutical industry. Therefore, much effort has been directed to partially oxidize CH<sub>4</sub>. For low temperature conditions, the conversion processes can be classified into electrochemical process,<sup>[74]</sup> photocatalysis,<sup>[75,76]</sup> enzyme catalysis,<sup>[77–79]</sup> chemical catalysis or reagent process,<sup>[80,81]</sup> and liquid phase

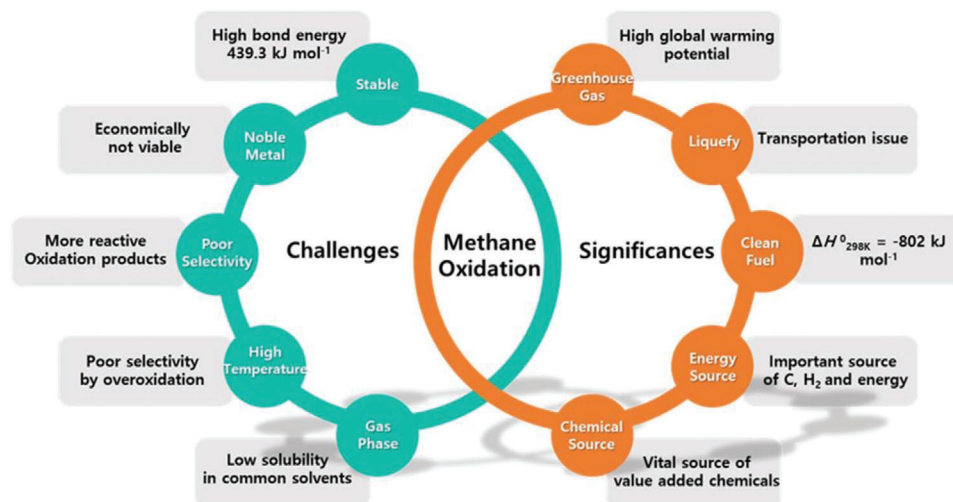


Figure 4. Challenges and significances of CH<sub>4</sub> oxidation.

oxidation (employing hydrogen peroxide).<sup>[55]</sup> After comprehensive comparison, electrochemical and photocatalytic processes have performed promising prospect for industrial application at low temperatures, which will be described in details in the following sections.

### 3.1. Electrochemical Processes

Electrochemistry is a powerful technique to control redox reactions through the precise bias application, offering electrochemical oxidation as an economical alternative route to chemical conversion processes.<sup>[82–84]</sup> The advantages of the electrochemical processes could be summarized as, i) relatively low cost (neglecting the initial cost of the equipment, power is generally less expensive than chemical reagents) with adequate yield,<sup>[85]</sup> ii) usually occurring under ambient conditions with low temperatures ( $\leq 100$  °C),<sup>[86,87]</sup> iii) convenient for scaling up,<sup>[21,88]</sup> and iv) satisfaction of most principles for green chemistry.<sup>[89,90]</sup> More importantly, in electrochemical process, kinetics and therefore the rate of product generation and their selectivity can be controlled by monitoring the applied potential.<sup>[91]</sup> In contrary, thermal conversion of methane (reforming of methane) occurs at high temperatures ( $> \approx 700$  °C) that impart several challenges as discussed in Section 2.2. Moreover, at high temperatures catalyst degrades rapidly due to coking<sup>[92]</sup> and catalyst sintering, and greenhouse gas emission occurs.<sup>[93]</sup> On the other hand, enzymatic oxidation (e.g., by methane monooxygenases) of methane to methanol occurs under ambient conditions in the presence of O<sub>2</sub>.<sup>[94]</sup> However, such oxidation suffers from poor kinetics and low carbon and energy efficiencies.<sup>[95]</sup> Moreover, these enzymes themselves are usually slow and complex. Over the last decades, electrochemical oxidation of CH<sub>4</sub> has been a topic of principal interest.<sup>[96]</sup> Electrochemical CH<sub>4</sub> oxidation is thermodynamically favorable at modest potentials (e.g., CH<sub>4</sub> (g) + H<sub>2</sub>O (l) → CH<sub>3</sub>OH (aq) + 2H<sup>+</sup> + 2e<sup>-</sup> reaction has  $E^0 = 0.586$  V versus normal hydrogen electrode (NHE) at pH = 0 and 298 K), but kinetically sluggish, which could be improved with the high overpotential assis-

Table 1. Methane oxidation to oxygenates and the respective potentials. The data were adapted with permission;<sup>[97]</sup> (aq) indicates aqueous solution.

Methane oxidation reaction	$E$ (V vs RHE)
CH <sub>4</sub> (g) + H <sub>2</sub> O (l) → CH <sub>3</sub> OH (aq) + 2H <sup>+</sup> (aq) + 2e <sup>-</sup>	0.58
CH <sub>4</sub> (g) + H <sub>2</sub> O (l) → HCHO (aq) + 4H <sup>+</sup> (aq) + 4e <sup>-</sup>	0.46
CH <sub>4</sub> (g) + H <sub>2</sub> O (l) → HCOOH (aq) + 6H <sup>+</sup> (aq) + 6e <sup>-</sup>	0.26
CH <sub>4</sub> (g) + H <sub>2</sub> O (l) → CO (g) + 6H <sup>+</sup> (aq) + 6e <sup>-</sup>	0.26
CH <sub>4</sub> (g) + H <sub>2</sub> O (l) → CO <sub>2</sub> (g) + 8H <sup>+</sup> (aq) + 8e <sup>-</sup>	0.17

tance for proceeding at low temperatures (Table 1).<sup>[97]</sup> However, at high overpotentials (especially at  $\geq 0.8$  V vs reversible hydrogen electrode (RHE)), water oxidation (oxygen evolution) undergoes at high rate,<sup>[98,99]</sup> resulting in extra energy loss as well as increased cost of CH<sub>4</sub> oxidation significantly. In the electrochemical processes, either oxygen site on the electrode surface or free radicals at the electrode/electrolyte interface can activate CH<sub>4</sub> at ambient temperatures.<sup>[91]</sup> Schematic diagram of an electrochemical cell for CH<sub>4</sub> oxidation is presented in Figure 5. It consists of three main parts: i) an anode, where CH<sub>4</sub> oxidation occurs; ii) a cathode, where the reduction half-reaction takes place; and iii) an electrolyte, an ion conducting medium that separates the two electrodes. The anode and cathode are connected through an external circuit. However, in this process selective production of a desired product is challenging as the electrode potential values of different products are often very close and high reactivity of free radicals and reactive oxygen species.<sup>[100]</sup>

In the following few paragraphs we will discuss fundamental parameters that play important role in CH<sub>4</sub> electrooxidation reactions.

**Onset potential:** It is an intrinsic property of any electrocatalytic reaction. Ideally, onset potential of a reaction should be equal to its equilibrium potential. However, in practice onset potential is usually much greater than the equilibrium potential, as any electrode reaction occurs only after surmounting the

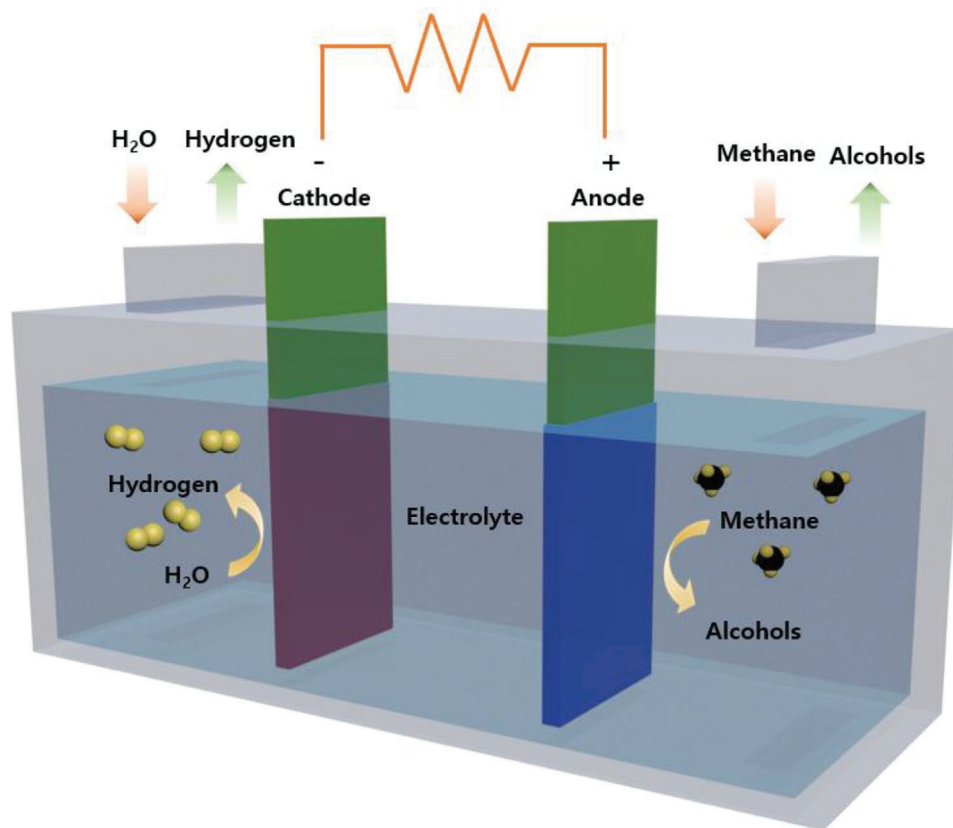


Figure 5. Diagram of an electrochemical cell for  $\text{CH}_4$  oxidation to alcohols.

electrode kinetic energy barrier. It is often difficult to find out the exact value of onset potential. Therefore, often it is measured at a particular current density, e.g.,  $1 \text{ mA cm}^{-2}$ .

Current density: It is an important parameter to measure the efficiency of a catalyst. It is usually expressed as  $\text{mA cm}^{-2}$ . However, current density could be measured by the unit mass of the catalyst on the electrode surface.

Faradaic efficiency (FE): Faradaic efficiency or current efficiency is the efficiency with which electrons carry out a desired electrochemical reaction. It can be calculated by the following equation.  $\text{FE}(\%) = \frac{\alpha n F}{Q}$ , where,  $\alpha$  is the number of electrons transferred in a desired electrochemical reaction and  $n$  is the number of mole(s) of the product formed (e.g., for MeOH production from  $\text{CH}_4$ ,  $\alpha$  is 2 and  $n$  is 1, see Table 1),  $F$  is the Faraday constant,  $96485 \text{ C mol}^{-1}$ , and  $Q$  is the number of charge passed. Faradaic efficiency is a measure of product selectivity.

### 3.1.1. Electrochemical Systems for $\text{CH}_4$ Oxidation

Most conversion processes at low temperatures are ideal and feasible because the energy input is low and reaction conditions can be easily achieved and maintained. Table 2 summarizes literatures for electrochemical  $\text{CH}_4$  oxidation at low temperatures. In early studies, electrocatalytic  $\text{CH}_4$  oxidation were carried out on platinum electrodes at an appreciable rate in aqueous phosphoric, sulfuric and perchloric acid at  $60\text{--}150 \text{ }^\circ\text{C}$ .<sup>[101–104]</sup> However,

noble metal Pt restricts its wide applications. Fortunately, Frese replaced Pt by gold, glassy carbon, copper and mercury cathodes for partial oxidation of  $\text{CH}_4$  in different aqueous electrolytes (e.g.,  $0.01\text{--}2 \text{ M KOH}$ ,  $2 \text{ M NaOH}$ , and  $0.1 \text{ M NaClO}_4$  solution) containing dissolved oxygen in the potential range of  $0.8\text{--}0.4 \text{ V}$  (vs dynamic hydrogen electrode) at  $25 \text{ }^\circ\text{C}$ .<sup>[105]</sup> The main oxidation product was formaldehyde, although a little amount of methanol was produced in some experiments. These products were generated at high rates due to the reactive oxygen species (e.g.,  $\text{O}_2^-$  or  $\text{O}_2\text{H}^-$ ) that were formed as a stable intermediate by electrochemical reduction of oxygen.

For avoiding the toxic materials, Qiao et al. demonstrated electrocatalytic  $\text{CH}_4$  oxidation over multiwalled carbon nanotube-Nafion/nickel hydroxide-modified nickel electrodes in  $1.0 \text{ M NaOH}$  solution.<sup>[106]</sup> A linear relationship could be observed between the oxidation peak current and the concentration of  $\text{CH}_4$ , which indicated that  $\text{CH}_4$  was effectively oxidized to methanol by NiOOH electrocatalyst. In an interesting work focusing on the electrode design, Rocha et al. developed a gas diffusion electrode (GDE) for the selective methanol electro-synthesis from  $\text{CH}_4$  on a  $\text{V}_2\text{O}_5$  incorporated  $\text{TiO}_2/\text{RuO}_2$ /polytetrafluoroethylene (PTFE) electrode.<sup>[107]</sup> Formaldehyde and formic acid were synthesized at the similar rate making the process poor selective for methanol formation. Nevertheless, increasing potential increased the amount of methanol, which reached at a maximum of 30% current efficiency at  $2.2 \text{ V}$  versus saturated calomel electrode (SCE). In a follow up work, the same group reported that

**Table 2.** Summaries of electrocatalytic CH<sub>4</sub> oxidation systems at low temperatures.

Catalyst	T [°C]	Oxidant	Electrolyte [M]	Potential [V]	Products	Mechanism
Au, glassy carbon, Hg, Cu	25	O <sub>2</sub>	KOH (0.01–2), NaOH (2), NaClO <sub>4</sub> (0.1)	0.8–0.4 (DHE) <sup>a)</sup>	HCHO, MeOH, CO and CO <sub>2</sub>	Radical <sup>[105]</sup>
CNT/Nafion/Ni(OH) <sub>2</sub> /Ni <sup>b)</sup>	RT	NaOH	NaOH (1.0)	0.27 (Ag/AgCl)	MeOH	[106]
TiO <sub>2</sub> /RuO <sub>2</sub> /PTFE/V <sub>2</sub> O <sub>5</sub> <sup>c)</sup>	RT	RuO <sub>2</sub> /V <sub>2</sub> O <sub>5</sub>	Na <sub>2</sub> SO <sub>4</sub> (0.2)	2.0 (SCE)	MeOH, HCHO, HCOOH	Radical <sup>[108]</sup>
NiO–ZrO <sub>2</sub>	RT	CO <sub>3</sub> <sup>2-</sup>	Na <sub>2</sub> CO <sub>3</sub> (0.1)	0.5–0.6 (SCE)	MeOH, EtOH, CO, Pr <sup>i</sup> OH, CH <sub>3</sub> COCH <sub>3</sub>	[74]
Pt	RT	Cl <sub>2</sub>	KCl (0.6)	1.0–1.3 (SCE), Hg lamp	MeOH, CH <sub>3</sub> Cl, CH <sub>2</sub> Cl <sub>2</sub> , CHCl <sub>3</sub>	Radical <sup>[109]</sup>
Pt	RT	Cl <sup>-</sup>	KCl (pH 11)	1.3 (SCE)	MeOH, CH <sub>3</sub> Cl	Radical <sup>[110]</sup>
Co <sub>3</sub> O <sub>4</sub> /ZrO <sub>2</sub>	RT	CO <sub>3</sub> <sup>2-</sup>	Na <sub>2</sub> CO <sub>3</sub> (0.5)	2.0	MeOH, HCHO, EtOH, PrOH, CH <sub>3</sub> CHO	Radical <sup>[111]</sup>
Pt/C, Pt/C-ATO, Pd/C, Pd/C-ATO <sup>d)</sup>	25, 80	ATO	H <sub>2</sub> SO <sub>4</sub> (0.5)	0.9 (RHE)	CO <sub>2</sub>	[112]
Pd-black/VO(acac) <sub>2</sub> -VGCF cathode <sup>e)</sup>	25	O <sub>2</sub>	H <sub>3</sub> PO <sub>4</sub> (1)	0.65 V	CO <sub>2</sub>	Radical <sup>[113,114]</sup>
V <sub>2</sub> O <sub>5</sub> /SnO <sub>2</sub> anode	100	H <sub>2</sub> O	Sn <sub>0.9</sub> In <sub>0.1</sub> P <sub>2</sub> O <sub>7</sub>	900 mV	MeOH	Radical <sup>[115]</sup>
ZrO <sub>2</sub> :NiCo <sub>2</sub> O <sub>4</sub>	25	CO <sub>3</sub> <sup>2-</sup>	0.5 M Na <sub>2</sub> CO <sub>3</sub>	2.0	PrOOH, AcOH, <sup>f)</sup> acetone	[116]
NiO/Ni	25	NaOH	0.1 M NaOH	1.40 (RHE)	EtOH	[117]
NiO@Ni hollow fiber	25	NaOH	0.1 M NaOH	1.46 (RHE)	MeOH and EtOH	[118]

<sup>a)</sup> Dynamic hydrogen electrode; <sup>b)</sup> Multiwalled carbon nanotube; <sup>c)</sup> Polytetrafluoroethylene; <sup>d)</sup> Antimony-doped tin oxide; <sup>e)</sup> Vertically grown carbon nanofiber; <sup>f)</sup> Acetic acid.

incorporation of V<sub>2</sub>O<sub>5</sub> into TiO<sub>2</sub>/RuO<sub>2</sub>/PTFE GDE suppressed the formation of formaldehyde and formic acid, thereby increased MeOH selectivity.<sup>[108]</sup> A 5.6 wt% V<sub>2</sub>O<sub>5</sub> loading to the GDE increased the current efficiency of the electrode to 57% at 2.0 V versus SCE. In the catalytic process, CH<sub>4</sub> was first transformed to methyl bisulfate (by the supporting electrolyte, Na<sub>2</sub>SO<sub>4</sub>), which was then hydrolyzed to methanol by the vanadium redox couples. The electrocatalytic experiment was carried out for 1 h. However, the catalyst stability was not reported.

### 3.1.2. Electrolyte Mediated CH<sub>4</sub> Oxidation

Hydroxide ions are conventionally used in the electrochemical CH<sub>4</sub> oxidation as alkaline medium, which not only serve the purpose of a base but also act as an oxidizing agent. Unfortunately, OH<sup>-</sup> ions do not have enough oxidizing ability to abstract protons from the unusually strong C–H bonds in CH<sub>4</sub>, especially at low temperatures. This is the reason for which CH<sub>4</sub> oxidation in hydroxide media does not show appreciable activity.<sup>[119]</sup> Therefore, Spinner and Mustain reported electrochemical CH<sub>4</sub> activation in Na<sub>2</sub>CO<sub>3</sub> (0.1 M) aqueous solution at room temperature on a NiO–ZrO<sub>2</sub> composite catalyst.<sup>[74,120]</sup> The carbonate ions were adsorbed on the nonconducting ZrO<sub>2</sub>, while CH<sub>4</sub> was adsorbed and activated by NiO. Oxygen ions were then abstracted from the carbonate ions and donated to the electrochemically active sites to make new bonds with carbon or hydrogen in CH<sub>4</sub>. It is interesting to note that, unlike OH<sup>-</sup> ions, CO<sub>3</sub><sup>2-</sup> ions donate oxygen ions with successive release of CO<sub>2</sub>, which generated a large change in the enthalpy of reaction, favoring oxidation kinetics even at low temperatures.<sup>[111]</sup> Additionally, the presence of the redox couple Ni<sup>2+</sup>/Ni<sup>3+</sup> (by the reaction, Ni(OH)<sub>2</sub> + OH<sup>-</sup> ↔ NiOOH + H<sub>2</sub>O + e<sup>-</sup>) at 0.5–0.6 V vs SCE favored the oxidation process. The products were identified as different oxygenates, such as methanol, ethanol, isopropanol, formaldehyde, formate,

acetate, acetone, and carbon monoxide. Oxygen and carbon dioxide were also formed slightly from the electrolysis of carbonate ions and/or the oxygen evolution reaction, which was catalyzed by NiOOH above 0.85 V vs SCE (by the reaction 4OH<sup>-</sup> → O<sub>2</sub> + 2H<sub>2</sub>O + 4e<sup>-</sup>). **Figure 6** shows the CV and *iR*-corrected Nyquist plots for the electrooxidation on the NiO–ZrO<sub>2</sub> composite catalyst in N<sub>2</sub>- and CH<sub>4</sub>-saturated CO<sub>3</sub><sup>2-</sup> solutions. The increased current density and decreased resistance (≈87%) in the CH<sub>4</sub>-saturated electrolyte compared to the N<sub>2</sub>-saturated one demonstrated the CH<sub>4</sub> oxidation (**Figure 6a,b**). The authors assumed that the Ni<sup>3+</sup> species (NiOOH) was responsible for the oxidation of the intermediate oxygenates.<sup>[120–122]</sup> **Figure 6c,d** shows the proposed mechanism for the formation of methanol and the C–C bonds in ethanol, respectively. Interestingly, in this work new C–C bonds were formed. The suggested reaction pathways for the formation of different products are depicted in **Figure 6e**. The electrochemical device constructed is displayed in **Figure 6f**. In a closely related work, Mustain and co-workers, demonstrated the essential role of ZrO<sub>2</sub> for CH<sub>4</sub> conversion in a low temperature electrochemical process with the carbonate cells and proved that carbonate ions donated oxygen ions.<sup>[123]</sup> In contrast, with hydroxide-based cells, the catalyst nickel oxyhydroxide itself functions as an oxygen donor for the CH<sub>4</sub> conversion reaction.

Following the idea of Spinner, Park's group recently designed ZrO<sub>2</sub>/Co<sub>3</sub>O<sub>4</sub> composite catalysts for the electrochemical oxidation of CH<sub>4</sub> at room temperature.<sup>[111]</sup> A series of composite catalysts were synthesized with different ratios of Co<sub>3</sub>O<sub>4</sub> and ZrO<sub>2</sub>. Electron microscopy (**Figure 7**) images revealed that oval-shaped and uniform ZrO<sub>2</sub> nanoparticles were anchored on the surface of Co<sub>3</sub>O<sub>4</sub> nanoplates to make heterojunctions. Linear sweep voltammetry (LSV) curves (**Figure 8a,b**) proved that the 1–4 ZrO<sub>2</sub>/Co<sub>3</sub>O<sub>4</sub> electrocatalyst displayed the highest current density for CH<sub>4</sub> oxidation. Long-term electrochemical oxidation (at 2.0 V applied potential in a closed vessel containing 0.5 M Na<sub>2</sub>CO<sub>3</sub>, catalysts deposited on carbon paper working electrode and Pt foil counter

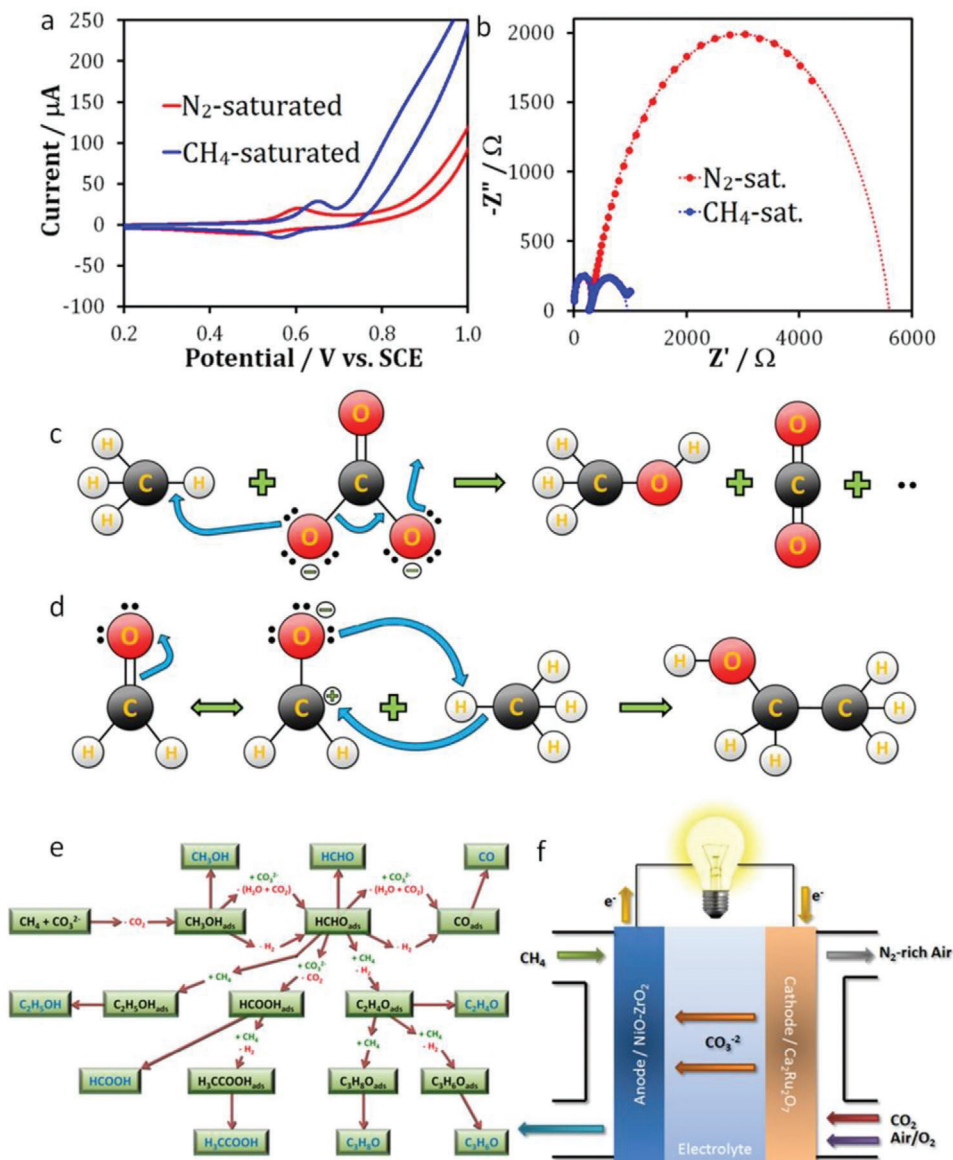


**Figure 6.** a) Cyclic voltammograms and b)  $iR$ -corrected Nyquist plots for  $N_2$ - and  $CH_4$ -saturated 0.1 M  $Na_2CO_3$  solution over a  $NiO-ZrO_2$  electrocatalyst. c) Reaction mechanism for the formation of methanol from  $CH_4$  and carbonate ions. d) Formation of the C-C bond in ethanol. e) Proposed reaction pathways for the activation of  $CH_4$  by carbonate ions. f) The electrochemical cell that was constructed in this work. Reproduced with permission.<sup>[74]</sup> Copyright 2013, The Electrochemical Society.

electrode) led to the formation of 1-propanol and 2-propanol as the main products, with production efficiency of >60% after 12 h of oxidation. Acetaldehyde was the key intermediate from which 1-propanol and 2-propanol were generated (Figure 8c and d<sub>3</sub>).  $CH_3OH$ ,  $C_2H_5OH$ ,  $CH_3CHO$ , and  $CH_3COCH_3$  were formed as byproducts. Notably, except methanol, all the products formed in this work were C3 species, which indicated the upgradation from an inert C1 starting material to higher-value organics. The electrochemical device for methane oxidation is displayed in Figure 8e. Moreover, replacing  $Co_3O_4$  in the previous system with a bimetallic oxide of  $NiCo_2O_4$ , Ma et al. described partial oxidation of  $CH_4$  to produce only C3 products – propionic acid, acetic acid and acetone with  $CH_4$  conversion efficiency of 47.5% after

20 h of reaction at room temperature.<sup>[116]</sup> The selectivity for propionic acid was calculated to be  $\approx 65\%$  with a rate of formation of  $1173 \mu mol g^{-1} h^{-1}$  after 20 h.

Recently, Song et al. engineered the interface of  $NiO/Ni$  by calcination and observed efficient electrooxidation of methane and C-C coupling in 0.1 M  $NaOH$  solution to produce ethanol under ambient conditions.<sup>[117]</sup> The FE of ethanol production and yield were reported to be 89% and  $25 \mu mol g_{NiO}^{-1} h^{-1}$ , respectively, by 3.0  $NiO/Ni$  electrocatalyst at 1.40 V versus RHE. The catalyst maintained nearly same current density for 24 h at 1.40 V versus RHE with a slight decrease in FE for EtOH production. X-ray photoelectron spectroscopy (XPS) analysis showed that  $NiO/Ni$  ratio was the same before and after 24 h of catalysis. Density functional

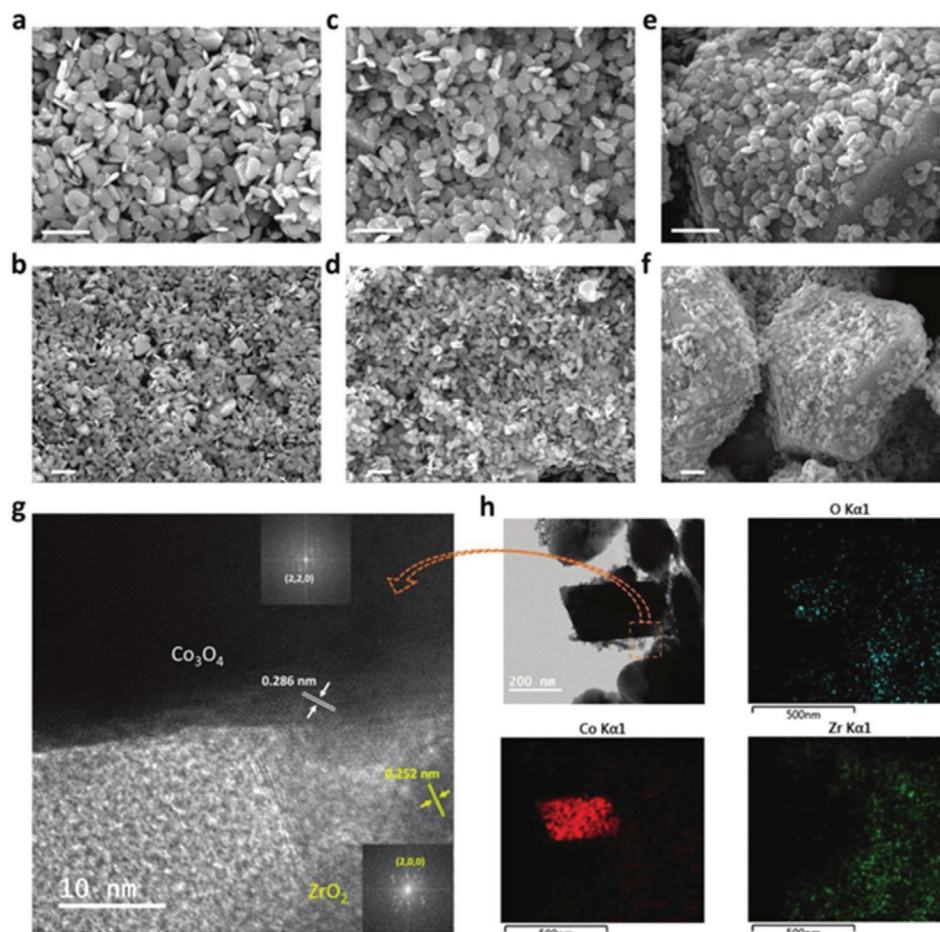


**Figure 7.** SEM micrographs of the a,b) 1–2 ZrO<sub>2</sub>/Co<sub>3</sub>O<sub>4</sub>, c,d) 1–4 ZrO<sub>2</sub>/Co<sub>3</sub>O<sub>4</sub>, and e,f) 1–6 ZrO<sub>2</sub>/Co<sub>3</sub>O<sub>4</sub> electrocatalysts. The scale bars in (a–f) are 1 μm. g) High-resolution (HR)-TEM image. The insets in (g) are fast Fourier transform patterns. h) TEM micrograph and elemental mappings of O, Co, and Zr in the 1–4 ZrO<sub>2</sub>/Co<sub>3</sub>O<sub>4</sub> electrocatalyst. Reproduced with permission.<sup>[111]</sup> Copyright 2017, Wiley-VCH GmbH.

theory (DFT) calculations explained highly selective ethanol formation that involved the following steps: CH<sub>4</sub>\* → CH<sub>3</sub>\* + H\*, CH<sub>3</sub>\* → CH<sub>2</sub>\* + H\*, CH<sub>2</sub>\* + OH\* → CH<sub>2</sub>OH\* and CH<sub>3</sub>\* + CH<sub>2</sub>OH\* → CH<sub>3</sub>CH<sub>2</sub>OH\*, here \* denotes active site on the catalyst surface. On the other hand, Guo et al. demonstrated electrocatalytic methane oxidation over NiO@Ni hollow fiber (HF) in 0.1 M NaOH aqueous solution under ambient conditions.<sup>[118]</sup> It was observed that the electrocatalyst 1%NiO@NiHF was able to achieve a FE for methanol production to 54% at 1.44 V (vs RHE), whereas the FE reached to 85% at 1.46 V for ethanol generation. The electrocatalyst was stable for 3 h.

### 3.1.3. Electrochemical Mechanism for CH<sub>4</sub> Oxidation

Selective oxidation of CH<sub>4</sub> is very important for providing desired products. In many of such oxidation reactions, electrochemically activated oxygen species (O\*) act as oxidizing agent. Appropriate cathodes can reductively activate O<sub>2</sub> molecules to generate O\* (O<sub>2</sub> + 2H<sup>+</sup> + 2e<sup>-</sup> + M<sup>n+</sup> → O\*–M<sup>n+</sup> + H<sub>2</sub>O, where M<sup>n+</sup> is the active site on the cathode, such as Sm<sup>3+</sup>, Fe<sup>3+</sup>, and Cu<sup>2+</sup>). The O\* can selectively oxidize light hydrocarbons to the correspond-

ing oxygenates (O\* + R–H → R–OH). This idea was adopted by Otsuka and Yamanaka, who reported selective oxidation of CH<sub>4</sub> at 28 °C on carbon whisker cathode.<sup>[113]</sup> However, it was speculated that the •OH oxidized CH<sub>4</sub> completely to CO<sub>2</sub> at near room temperature. Later, although this idea was further improved by the same group but the O\* was not potent enough to oxidize methane.<sup>[113,114]</sup> Nevertheless, the idea of electrochemically activated oxygen species was distinctive. This idea was further developed by Hibino and co-workers.<sup>[124]</sup> They demonstrated CH<sub>4</sub> oxidation to selectively produce methanol in a hydrogen–oxygen fuel cell that contained Sn<sub>0.9</sub>In<sub>0.1</sub>P<sub>2</sub>O<sub>7</sub> as electrolyte, which showed the capability for high proton conductivities above 80 °C, and Pd/C, Pt/C, Rh/C, Au/C, and PdAu/C (10 wt% metal basis) composites as cathodes (O<sub>2</sub> + 2H<sup>+</sup> + 2e<sup>-</sup> → O\* + H<sub>2</sub>O), and commercial Pt/C (60 wt% Pt) as anode (H<sub>2</sub> → 2H<sup>+</sup> + 2e<sup>-</sup>). The cathode was fed with methane and O<sub>2</sub> (50 vol% each) gas mixture, whereas the anode was provided with hydrogen. Notably, small quantity of hydrogen permeated from anode, through the electrolyte, to the cathode, where it reacted with the oxygen present therein. Then, O\* reacted with methane to produce methanol (O\* + CH<sub>4</sub> → CH<sub>3</sub>OH). The Pd/C catalyst was able to directly produce methanol from CH<sub>4</sub>, but the formation rate was not



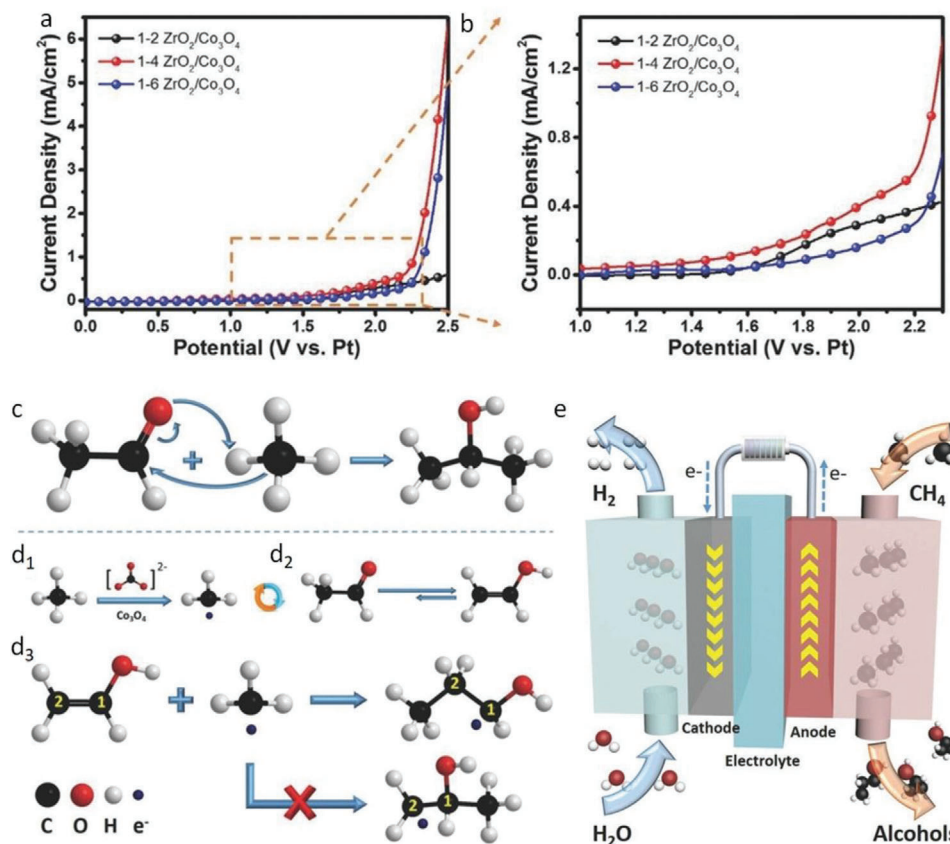
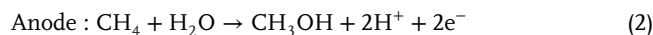
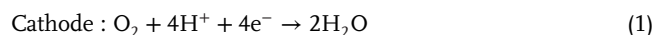


**Figure 8.** a,b) LSV curves of the ZrO<sub>2</sub>/Co<sub>3</sub>O<sub>4</sub> samples with the ratios of 1:2, 1:4, and 1:6 and their magnification, respectively. c) Nucleophilic addition reaction of methane to acetaldehyde to produce 2-propanol. d<sub>1</sub>–d<sub>3</sub>) Free radical addition reaction of methane to acetaldehyde to generate 1-propanol. e) The electrochemical device for methane oxidation. Reproduced with permission.<sup>[111]</sup> Copyright 2017, Wiley-VCH GmbH.

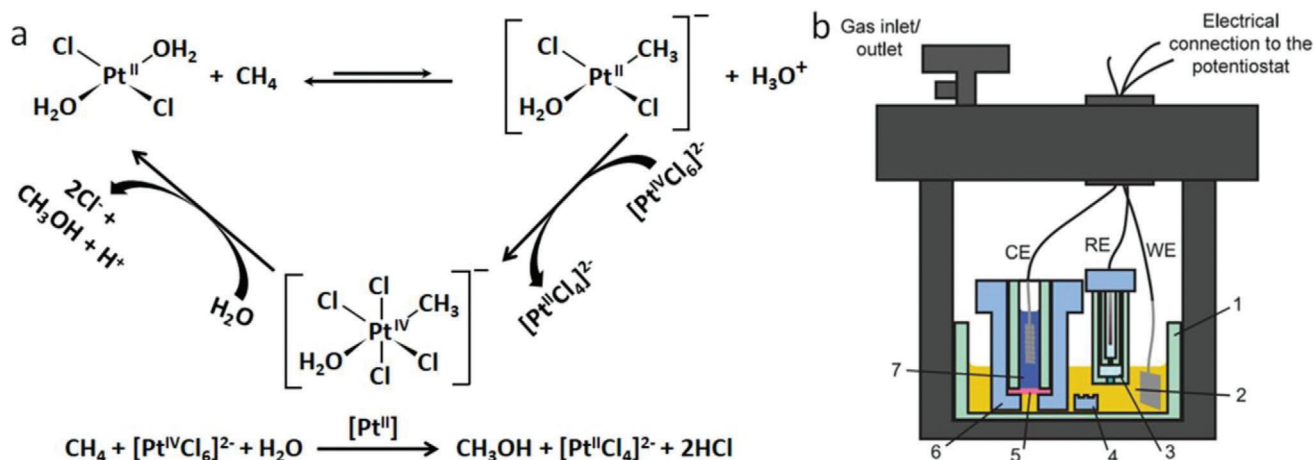
satisfactory. In contrast, the Pt/C and Au/C cathodes catalyzed the formation of CO<sub>2</sub>. The Rh/C cathode displayed practically insignificant catalytic activity for methane oxidation; the bimetallic Pd/Au cathode (at a ratio of 8:1) demonstrated the highest rate of methanol formation. The selectivity for methanol formation reached 60.0% at a current efficiency for CH<sub>4</sub> conversion of merely 0.012% at 50 °C, with CO<sub>2</sub> as the minor product. Furthermore, with the temperature increased, the selectivity toward methanol decreased, although the rate of conversion was higher. The authors speculated the possibility of electrochemical generation of H<sub>2</sub>O<sub>2</sub> or its derivatives at the cathodes. Interested readers are suggested to go through the reference for the details.

Although these works showed a new direction for the direct and selective oxidation of CH<sub>4</sub> to produce methanol at low temperatures, the current efficiency for the conversion was very low (merely 0.012%). The dominant reaction occurred at the cathode was water production (2H<sup>+</sup> + 2e<sup>-</sup> + 0.5O<sub>2</sub> → H<sub>2</sub>O), instead of O\* generation. This challenge was further overcome by Hibino and Lee, through carrying out CH<sub>4</sub> oxidation at the anode instead of cathode in a fuel cell-type reactor at low temperatures.<sup>[115]</sup> At the anode, a mixture of CH<sub>4</sub> and water vapor was supplied, whereas air was provided to the cathode. Several catalysts were used as anodes. However, a significant amount of methanol was produced on the V<sub>2</sub>O<sub>5</sub>/SnO<sub>2</sub> anode using Sn<sub>0.9</sub>In<sub>0.1</sub>P<sub>2</sub>O<sub>7</sub> proton conductor as the electrolyte at 100 °C. Unfortunately, the identification of O\*

was not clear to the authors. However, different reactive oxygen species O\*<sup>-</sup> (H<sub>2</sub>O → O\*<sup>-</sup> + 2H<sup>+</sup> + e<sup>-</sup>) and O<sub>2</sub>\*<sup>-</sup> (2H<sub>2</sub>O → O<sub>2</sub>\*<sup>-</sup> + 4H<sup>+</sup> + 3e<sup>-</sup>) were formed electrochemically over V<sup>4+</sup> sites. The maximum current efficiency for methanol production was determined to be 61.4%, and the selectivity was calculated to be 88.4% at 100 °C and at ≈900 mV (measured with a Hokuto Denko HE-101 electrometer). The reactions that occurred at the electrodes are given below



In a different approach, Ogura and Takamagari combined photochemical and electrochemical oxidation of CH<sub>4</sub> at room temperature.<sup>[109]</sup> A Pt plate was used as anode in a 0.6 M KCl solution of 11.0 pH and a low pressure mercury lamp (4 W) as an illuminator (254 nm). The applied potential was varied from 1.0 to 1.3 V (vs SCE). Depending on the potential applied, the products generated were methyl chloride, methanol, methylene dichloride and a small amount of trichloromethane. Following the same approach, this group further reported the realization of methanol and methyl chloride from CH<sub>4</sub> at room temperature.<sup>[110]</sup> The process involved was electrochemical oxidation of chloride ions to



**Scheme 1.** a) Shilov cycle and overall chemical reaction for electrochemical selective oxidation of methane to methanol. b) The diagram of the electrochemical cell used for methane oxidation by Surendranath et al. WE: working electrode, Pt foil; RE: reference electrode, Ag/AgCl; CE: counter electrode, Pt mesh. 1: glass cell; 2: reaction solution containing Pt salt; 3: fritted tube for making room of RE; 4: PTFE stir bar; 5: H<sup>+</sup> ion conducting membrane; 6: PTFE body holding the membrane stack and 7: counter electrode compartment containing sacrificial electron acceptor VOSO<sub>4</sub> (3 M). The WE compartment contained  $3 \times 10^{-3}$  M K<sub>2</sub>PtCl<sub>4</sub>,  $7 \times 10^{-3}$  M Na<sub>2</sub>PtCl<sub>6</sub>·6H<sub>2</sub>O,  $10 \times 10^{-3}$  M NaCl, and 0.5 M H<sub>2</sub>SO<sub>4</sub>. The cell and solution were O<sub>2</sub>-free and pressurized with CH<sub>4</sub> at 500 psi and the temperature was 130 °C. Reproduced with permission.<sup>[130]</sup> Copyright 2019, American Chemical Society (<https://pubs.acs.org/doi/10.1021/acscentsci.9b00273>, further permission related to the material excerpted should be directed to the ACS).

chlorine molecules, followed by the generation of chloride radicals upon light illumination, which triggered the activation of CH<sub>4</sub>. The main advantage of these works is that CH<sub>4</sub> was directly oxidized to methanol without further oxidation.

### 3.1.4. The Shilov Cycle

Another way to realize CH<sub>4</sub> oxidation is to use the Shilov cycle named after Alexander E. Shilov.<sup>[125–127]</sup> We will mention it here briefly for academic interest. The Shilov system is a classic example of C–H bond activation in which stronger C–H bonds preferentially undergo partial oxidation to the respective alcohol over the weaker ones. It is catalyzed by PtCl<sub>2</sub> in an aqueous solution, where PtCl<sub>6</sub><sup>2-</sup> acts as the ultimate oxidizing agent. In the first step, electrophilic addition of CH<sub>4</sub> (or an alkane) to the Pt(II) center of chloroplatinate occurs in an aqueous medium. Simultaneous deprotonation leads to the formation of a Pt(II)–CH<sub>3</sub> complex. In the second step, [Pt(IV)Cl<sub>6</sub>]<sup>2-</sup> oxidizes the Pt(II)–CH<sub>3</sub> complex to form the Pt(IV)–CH<sub>3</sub> complex. Subsequent nucleophilic attack by H<sub>2</sub>O molecules or Cl<sup>-</sup> ions at the methyl group of the Pt(IV)–CH<sub>3</sub> complex leads to the formation of methanol or methyl chloride (which is easily hydrolyzable to methanol), with simultaneous regeneration of the Pt(II).<sup>[128]</sup> A schematic of the Shilov cycle and the overall reaction are shown in **Scheme 1a**.

However, there is no practical application for CH<sub>4</sub> oxidation by this cycle. Fortunately, with water soluble *p*-toluenesulfonic acid (*p*-TsOH, 0.21 M) as a model substrate for CH<sub>4</sub> electrochemical oxidation was reported,<sup>[129]</sup> Liu and Nusrat realized electrocatalytic conversion of *p*-TsOH as a surrogate of CH<sub>4</sub> in 0.5 M H<sub>2</sub>SO<sub>4</sub> at about 560 mV (vs Ag/AgCl) applied potential with a homogeneous solution of Na<sub>2</sub>PtCl<sub>4</sub> as a Pt(II) catalyst,<sup>[128]</sup> expecting similar catalyst process for electrocatalytic CH<sub>4</sub> oxidation to methanol. Notably, the originally reported Shilov cycle suffers from the requirements of stoichiometric Pt(IV) that is

not economically viable. In this regard, recently Kim and Surendranath reported continuous regeneration of Pt(IV) through the electrochemical route.<sup>[130]</sup> It was noted that the metallic Pt electrode (with surface adsorbed Cl<sup>-</sup> ions) drove oxidation of Pt(II) through an inner sphere electron transfer mechanism (that involved transfer of the surface adsorbed Cl to Pt(II)) to form Pt(IV), at low overpotential. Thus by monitoring the potential of the Pt(II) catalyzed methane oxidation, the Pt(II)/Pt(IV) ratio was maintained resulting in continuous formation of methanol. The catalyst system was able to produce methanol for 30 h with selectivity for CH<sub>3</sub>OH and CH<sub>3</sub>Cl production of >80% (70% selectivity for CH<sub>3</sub>OH). It should be mentioned here that further oxidation of MeOH was suppressed by the presence of excess Cl<sup>-</sup> ions (from NaCl) that also maintained the Pt(II)/Pt(IV) concentration ratio. The methane oxidation reaction was performed at >100 °C in a home-built high-pressure two compartment electrochemical cell shown in the diagram in **Scheme 1b**.

### 3.2. Photocatalytic Oxidation of CH<sub>4</sub>

Photocatalysis is a widely studied technique for organic dye degradation and water purification including water decontamination and disinfection.<sup>[131,132]</sup> In a typical photocatalytic process, a semiconductor is excited with a light source to generate electron–hole pairs. The resultant electrons and holes possess kinetic energy equal to the bandgap value of the semiconductor. The electrons transport to the conduction band and perform reduction, whereas the holes occupy the valence band and execute oxidation.<sup>[133,134]</sup> A generalized photocatalytic process is depicted in **Figure 9a**. Photocatalysis enables difficult chemical reactions to occur at room/low temperatures. Therefore, this process offers low cost oxidation of methane and enhanced catalyst stability. In contrary, thermal and enzymatic methane oxidation confront several challenges as discussed in Section 3.1. For the photocatalytic

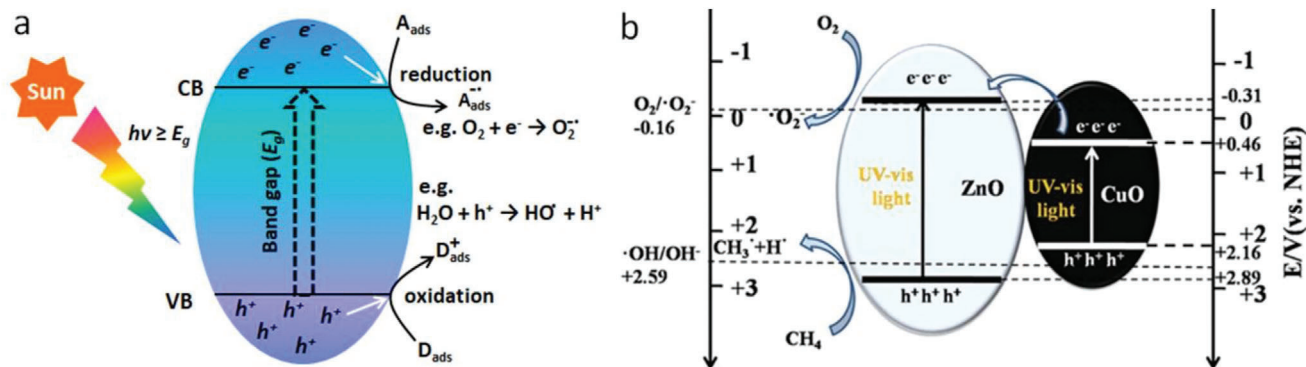


**Figure 9.** Generalized photocatalytic scheme a),  $A_{\text{ads}}$  and  $D_{\text{ads}}$  are, respectively, the adsorbed acceptor and adsorbed donor species over the photocatalyst. b) Bandgap positions of a photocatalyst to carry out  $\text{CH}_4$  oxidation with example of ZnO and CuO. Reproduced with permission.<sup>[143]</sup> Copyright 2019, The Royal Society of Chemistry.

oxidation of methane to occur, suitable photocatalysts are essential, in order to generate highly energetic oxygen species, such as  $\text{O}_2^-$  and  $\bullet\text{OH}$  radicals. Therefore, a photocatalyst must have a conduction band minimum more negative than the potential of the  $\text{O}_2/\text{O}_2^-$  redox couple ( $-0.16$  V vs normal hydrogen electrode, NHE) and a valence band maximum more positive than the potential of the  $\bullet\text{OH}/\text{OH}^-$  redox couple ( $+2.59$  V vs NHE) (Figure 9b).<sup>[135–137]</sup> As we mentioned earlier, we are not going to discuss the photocatalytic conversion of  $\text{CH}_4$  to higher alkanes. Interested readers are referred to the reviews.<sup>[21]</sup> Numerous photocatalysts have been investigated for  $\text{CH}_4$  oxidation.<sup>[138]</sup> In the following sections, we discuss different processes for the photocatalytic  $\text{CH}_4$  oxidation at low temperatures, summarized in Table 3.

### 3.2.1. Photocatalytic Conversion of $\text{CH}_4$ with $\text{O}_2$

Recently, photocatalytic partial oxidation of  $\text{CH}_4$  by oxygen to obtain products, such as methanol, formaldehyde, and CO, has been an interesting topic of research. However, the oxidation of  $\text{CH}_4$  by  $\text{O}_2$  is a spin-forbidden process because  $\text{CH}_4$  and its products (such as methanol) are in the singlet (ground) state, whereas oxygen is in the triplet electronic state.<sup>[138]</sup>

In 1978, for the first time,  $\text{CH}_4$  was photocatalytically converted by oxygen under UV light exposure on  $\text{V}/\text{SiO}_2$  and  $\text{TiO}_2$  and  $\gamma$  irradiation on  $\text{V}/\text{SiO}_2$  and  $\text{P}/\text{SiO}_2$  photocatalysts.<sup>[139]</sup> In each case, upon light exposure hole centers,  $\text{O}^-$  species were generated ( $\text{O}^{2-} + \text{h}^+ \rightarrow \text{O}^-$ ), which attacked  $\text{CH}_4$  to yield methyl radicals that ultimately formed methoxide ( $\text{CH}_3\text{O}^-$ ). Besides, CO,  $\text{C}_2\text{H}_6$ , and a trace amount of  $\text{CO}_2$  were produced (in the absence of  $\text{O}_2$  and at up to  $88$  °C) on  $\gamma$  irradiated  $\text{V}/\text{SiO}_2$ . Unfortunately, hazardous  $\gamma$  radiation was employed in this work. For further improvement, using  $\text{V}_2\text{O}_5$  ( $\text{V}_2\text{O}_5/\text{SiO}_2$ -IW (incipient wetness), 0.6 mol% V) instead of V led to the photooxidation of  $\text{CH}_4$  to produce formaldehyde (corresponding to 76 mol% selectivity and 0.48 mol% one-pass yield) under UV radiation ( $<310$  nm) at  $120$  °C after 2 h of reaction.<sup>[159]</sup> Both UV light and a temperature were essential for this reaction. A tetravalent vanadium (with  $\text{V} = \text{O}$ ) was excited by UV light forming a charge–transfer complex, wherein a positive hole was confined by an oxygen atom to produce a strongly electrophilic  $\text{O}^-$  radical ion species.  $\text{CH}_4$  was

adsorbed on the photoactivated species, which would activate the C–H bonds. Molecular  $\text{O}_2$  could be adsorbed at the electron rich site of the generated intermediate, which could abstract hydrogen to produce HCHO.  $\text{O}^-$  Centers were created by the charge–transfer excitation from O 2p to the metal valence d orbitals. The lifetime of the photogenerated electron–hole pairs was the decider for the activity of the  $\text{O}^-$  centers. The longer lifetime of the excited state provides more efficient  $\text{CH}_4$  photoexcitation by the  $\text{O}^-$  centers. For example, in  $\text{MoO}_3$ , the lifetime of the electron–hole excited state was determined to be  $63$   $\mu\text{s}$ , which could be increased by Cu doping.<sup>[160]</sup> Through theoretical, as well as, experimental studies, Ward et al. proved that Cu-doped  $\text{MoO}_3$  photocatalysts are more effective for heterolytic C–H bond activation than pristine  $\text{MoO}_3$ .<sup>[140]</sup> In this process,  $\text{CH}_4$  was partially oxidized to  $\text{CH}_3\text{OH}$  in the presence of  $\text{O}_2$  at  $100$  °C. Methanol formation rate was the maximum when the concentrations of Cu and Mo were equal. The Cu doping makes  $\text{MoO}_3$  (resulting in  $\text{CuMoO}_4$ ) visible light active due to the presence of empty and filled orbitals (Cu 3d and O 2p) in the bandgap region between the O 2p and Mo 4d orbitals. Thus, some holes were stabilized by the alternative pathway, resulting in an increased lifetime of the excited state and the  $\text{O}^-$  sites.

In a further improvement, Grätzel and co-workers reported activation of  $\text{CH}_4$  by  $\text{O}_2$  on different photocatalysts illuminated by a solar simulator at room temperature and atmospheric pressure.<sup>[141]</sup> Pure  $\text{TiO}_2$  led to the formation of  $\text{CO}_2$ . However, deposition of 4%  $\text{MoO}_3$  on  $\text{TiO}_2$  produced a mixture product of CO and  $\text{CO}_2$ . Interestingly, when  $\text{TiO}_2$  was loaded with both  $\text{MoO}_3$  and  $\text{H}_4\text{SiW}_{12}\text{O}_{40}$ , CO was the main product. Contrarily, only tungstosilicate ( $\text{SiW}_{12}\text{O}_{40}^{4-}$ )-loaded  $\text{TiO}_2$  activated  $\text{CH}_4$  to produce CO,  $\text{CO}_2$ , and  $\text{H}_2\text{O}$ .<sup>[142]</sup> To carry out photocatalysis in practical, sunlight is more desirable than solar simulator. In this endeavor, Krishna et al. used sunlight for room temperature photooxidation of  $\text{CH}_4$  in air by uranyl ions anchored within the mesopores of MCM-41 silicate.<sup>[161]</sup> The  $\text{UO}_2^{2+}$  ions were tightly attached to the silicate and caused the latter to absorb visible light.  $\text{CH}_4$  was converted 100% within 2.5 h. However, due to the long life and strongly oxidizing oxidation state of uranyl ions,  $\text{CO}_2$  was formed selectively.

An efficient photocatalyst would absorb the visible region (preferably) of the solar spectrum to generate more

**Table 3.** Summaries of low temperature photocatalytic processes for CH<sub>4</sub> oxidation.

Catalyst	T [°C]; P [Pa]	Light	Oxidant	Product [s]	Ref.
V/SiO <sub>2</sub> , TiO <sub>2</sub> , P/SiO <sub>2</sub>	RT	UV, γ	O <sub>2</sub>	CO <sub>2</sub>	[139]
Cu-doped MoO <sub>3</sub>	100	UV	O <sub>2</sub>	MeOH	[140]
TiO <sub>2</sub> , TiO <sub>2</sub> /MoO <sub>3</sub> , TiO <sub>2</sub> /MoO <sub>3</sub> /H <sub>4</sub> SiW <sub>12</sub> O <sub>40</sub>	RT	Solar simulator	O <sub>2</sub>	CO <sub>2</sub> , CO	[141]
TiO <sub>2</sub> /H <sub>4</sub> SiW <sub>12</sub> O <sub>40</sub>	RT	Solar simulator	O <sub>2</sub>	CO, CO <sub>2</sub> , H <sub>2</sub> O	[142]
UO <sub>2</sub> <sup>2+</sup> /MCM-41	RT	Sun	O <sub>2</sub>	CO <sub>2</sub>	[161]
ZnO and Ag/ZnO	RT	300 W Xe lamp	O <sub>2</sub>	CO <sub>2</sub>	[136]
CuO/ZnO	RT	Xe lamp	O <sub>2</sub>	CO <sub>2</sub>	[143]
Cu, La, Pt, Cu/La-doped WO <sub>3</sub>	98/10.1 m	UV/visible	H <sub>2</sub> O	MeOH, H <sub>2</sub>	[144]
Beta zeolites	RT	Deep UV	O <sub>2</sub>	MeOH	[145]
WO <sub>3</sub>	RT	Visible laser	H <sub>2</sub> O <sub>2</sub>	MeOH, CO <sub>2</sub> , O <sub>2</sub>	[146]
Ag <sup>+</sup> impregnated WO <sub>3</sub>	RT	355 nm laser	H <sub>2</sub> O	MeOH	[147]
Mesoporous WO <sub>3</sub>	55	Hg vapor lamp	H <sub>2</sub> O	MeOH	[148]
La-doped mesoporous WO <sub>3</sub>	55	UVC-visible	H <sub>2</sub> O	MeOH	[149]
MMT-modified TiO <sub>2</sub> <sup>a)</sup>	100	Hg lamp	CO <sub>2</sub>	CO, MeOH	[150]
CuPc-modified TiO <sub>2</sub> <sup>b)</sup>	RT	Visible light	CO <sub>2</sub>	CO, AcOH, CH <sub>3</sub> CHO	[151]
ZnS-ZnO	RT	UV-visible	CO <sub>2</sub>	–	[152]
Co-doped Al <sub>2</sub> O <sub>3</sub> /Co nanoparticles	RT	UV-visible-IR	CO <sub>2</sub>	CO, H <sub>2</sub>	[153]
Photochemical oxidation	<100	20 W low pressure Hg lamp	Water vapor	MeOH, AcOH, HCOOH, EtOH, acetone	[76]
Ru single atoms on Cu nanoparticles	RT	19.2 W cm <sup>-2</sup> white light illuminator	CO <sub>2</sub>	CO and H <sub>2</sub>	[92]
ZnO/La <sub>0.8</sub> Sr <sub>0.2</sub> CoO <sub>3</sub>	RT	Solar light	O <sub>2</sub>	CO <sub>2</sub> and H <sub>2</sub> O	[154]
FeOOH/m-WO <sub>3</sub>	RT	Visible light	H <sub>2</sub> O <sub>2</sub>	MeOH	[155]
Cocatalyst (Pt, Pd, Au or Ag)/ZnO	RT	Solar light	O <sub>2</sub>	MeOH and HCHO	[156]
Rh/SrTiO <sub>3</sub> <sup>c)</sup>	RT	UV light	CO <sub>2</sub>	CO and H <sub>2</sub>	[157]
BiVO <sub>4</sub> microcrystals	65	350 W Xe lamp	H <sub>2</sub> O	MeOH	[22]
0.33 metal wt% FeO <sub>x</sub> /TiO <sub>2</sub>	25	300 W Xe lamp	H <sub>2</sub> O <sub>2</sub>	MeOH	[158]

<sup>a)</sup> Montmorillonite; <sup>b)</sup> Phthalocyanine; <sup>c)</sup> Although the experiment was carried out at RT, the temperature of the catalyst reached to 300 °C, we mentioned this work as the temperature was generated from the irradiation, i.e., not applied from outside.

photogenerated charge carriers.<sup>[133]</sup> The loading of metal nanoparticles (especially noble metals) on the main photocatalysts often increases light absorption.<sup>[134]</sup> Recently, Chen et al. demonstrated high CH<sub>4</sub> oxidation activity of ZnO nanoparticles loaded with Ag nanoparticles under simulated sunlight.<sup>[162]</sup> The deposited Ag nanoparticles showed surface plasmon resonance and reduced recombination rate of the photogenerated charge carriers (Figure 10a), with faster surface reaction (Figure 10b) and increased visible light absorption (Figure 10c). A two-step mechanism for CH<sub>4</sub> oxidation was proposed (Figure 10d). In the first step, CH<sub>4</sub> reacted with oxygen to produce H<sub>2</sub>O and HCHO (CH<sub>4</sub> + O<sub>2</sub> → HCHO + H<sub>2</sub>O). HCHO, as the intermediate, reacted further with O<sub>2</sub> to produce CO<sub>2</sub> and H<sub>2</sub>O in the second step (HCHO + O<sub>2</sub> → CO<sub>2</sub> + H<sub>2</sub>O). The quantum yield of 8% was obtained at <400 nm wavelengths. The photocatalytic performance and photocatalyst remained unchanged after ten cycles, as shown in Figure 10e in a fixed-bed reactor revealed by the characterizations of X-ray diffraction (XRD), XPS, and optical absorption measurements. Moreover, it maintained its catalytic activity for 50 h in a flow-gas mode. Thus the photocatalyst was very stable for methane oxidation. Photocatalytic instruments in a fixed-bed reactor and flow-gas mode are represented in Figure 10f,g. For further development, Ag nanoparticles were replaced by in-

expensive CuO nanoparticles (<1 wt%), which resulted in more efficient CH<sub>4</sub> oxidation under ambient conditions.<sup>[143]</sup>

Notably, the band edge potential of CuO did not permit it to activate oxygen molecules (Figure 9b). Therefore, after excited to the conduction band of CuO, a fraction of the enriched electrons could be further excited to the conduction band of ZnO nanoparticles, satisfying sufficient energy to activate oxygen molecules (Figure 9b). The photoactivity of the catalyst system was very weak under the visible light illumination, as the electron transfer from CuO to ZnO was not easy under this condition. Nevertheless, this catalyst showed excellent stability for over a period of 450 min. Recently, Yang et al. demonstrated solar driven photocatalytic oxidation of methane at the epitaxial heterointerface of ZnO/La<sub>0.8</sub>Sr<sub>0.2</sub>CoO<sub>3</sub> to produce CO<sub>2</sub>.<sup>[155]</sup> The photothermal effect of the solar illumination boosted methane oxidation by ≈2 times by enhancing the electron transfer at the interface. Although these reports show considerable progress for CH<sub>4</sub> oxidation by molecular O<sub>2</sub>, technologically unimportant CO<sub>2</sub> was often generated. Achieving high catalytic activity and selectivity remained challenging, especially for partial oxidation products.

Nevertheless, co-catalyst (Pt, Pd, Au, or Ag) loaded ZnO oxidized CH<sub>4</sub> selectively to CH<sub>3</sub>OH and HCHO in the presence of molecular O<sub>2</sub> at room temperature in aqueous medium as

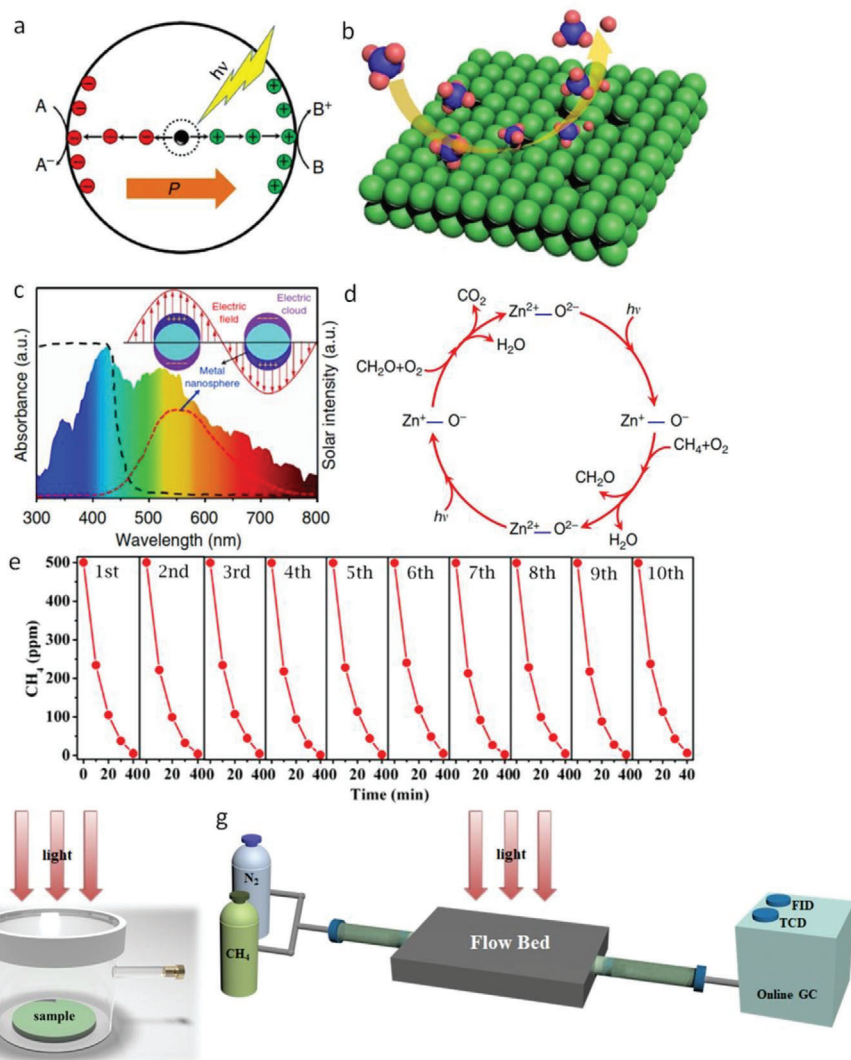


**Figure 10.** a) Polarity on photocatalyst induces fast charge separation and transport. b) Surface defects on photocatalyst leads to faster surface reaction. c) Surface decorated metal nanoparticles increases absorption of solar spectrum. d) Mechanism of photooxidation of methane. Stability of the catalyst for ten cycles. e) Schematic diagrams of photocatalytic instruments a) fixed-bed and b) flow-bed reactor that were used for photocatalytic methane conversion.<sup>[143,162]</sup> GC, FID, and TCD are gas chromatograph, flame ionization detector, and thermal conductivity detector, respectively. Reproduced with permission.<sup>[162]</sup> Copyright 2016, Springer Nature.

demonstrated by Song et al.<sup>[156]</sup> The photogenerated holes and electrons of the catalyst system activated CH<sub>4</sub> and molecular O<sub>2</sub> into •CH<sub>3</sub> and •OOH radicals, respectively, which subsequently converted to oxygenates. Notably, the mild reactive •OOH radicals stopped further oxidation of the oxygenates. Up to 250 μmol oxygenates, with ≈95% selectivity, were generated by 0.1 wt% Au loaded ZnO after 2 h of photocatalytic experiment. It should be pointed out here that compared to molecular O<sub>2</sub>; nitric oxide (NO) is a milder oxidizing agent that can oxidize CH<sub>4</sub> selectively to MeOH by a photocatalyst at room temperature.<sup>[163]</sup>

### 3.2.2. Photocatalytic Conversion of CH<sub>4</sub> with Water

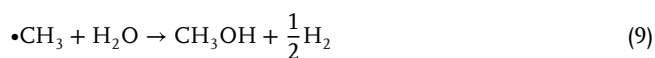
Direct conversion of CH<sub>4</sub> to oxygenates in the presence of steam (photocatalytic steam reforming of methane or SRM) via photo-

catalytic processes is of great significance. This conversion proceeds according to the following reaction:



Initial experiments of such process were carried out at the National Energy Technology Laboratory (Department of Energy, United States).<sup>[144,164]</sup> Taylor and co-workers converted CH<sub>4</sub> to methanol, hydrogen and acetic acid overdoped WO<sub>3</sub> (dopants were Cu, La, Pt and a mixture of Cu and La) photocatalysts at a temperature of ≈98 °C under atmospheric pressure.<sup>[164,165]</sup> Methyl viologen dichloride (1,1'-dimethyl-4,4'-bipyridinium dichloride, MV<sup>2+</sup>) hydrate was used as the electron transferring agent. Photolysis of water, overdoped WO<sub>3</sub> in the presence of MV<sup>2+</sup>, first generated hydroxyl radicals, which abstracted a hydrogen atom from CH<sub>4</sub> to produce methyl radicals.

Successively, the  $\bullet\text{CH}_3$  radicals reacted with water to form  $\text{CH}_3\text{OH}$ . Meanwhile, photocatalytic conversion of  $\text{CH}_4$  dissolved in water and methane hydrate overdoped  $\text{WO}_3$  and  $\text{TiO}_2$  photocatalysts in the presence of  $\text{MV}^{2+}$  was investigated.<sup>[144]</sup> The photoconversion of  $\text{CH}_4$  and methane hydrate was not successful below  $70^\circ\text{C}$  and 1.0 MPa. However, conversion occurred at  $50^\circ\text{C}$  under 10.1 MPa. Contrarily, methane hydrate underwent conversion at temperatures as low as  $-15^\circ\text{C}$ . The products did not depend on the pressure. It was further observed that  $\text{CH}_4$  conversion and methanol production increased with the addition of  $\text{H}_2\text{O}_2$ , suggesting involvement of hydroxyl radicals as an intermediate. L-doped  $\text{WO}_3$  showed the highest  $\text{CH}_4$  conversion efficiency. The main products were methanol and hydrogen. The general reaction pathway for these two works is given below. However, the generated methanol could possibly combine with holes to produce formic acid, carbon monoxide and carbon dioxide. This phenomenon indicated a selectivity challenge for this  $\text{CH}_4$  activation process. Moreover, the electron transfer agent, methyl viologen is a moderately expensive chemical.



Here,  $e_{\text{CB}}^-$  and  $h_{\text{VB}}^+$  represent electrons in the conduction band and holes in the valence band, respectively.

Interestingly, in the above works, methane hydrate was used with some special advantages. It contained much higher concentration of methane (15 mol%) than that can be obtained in a pressurized reactor containing  $\text{CH}_4$  and  $\text{H}_2\text{O}$ . Besides, methane hydrate provided the restricted mobility and close proximity of the  $\bullet\text{OH}$  radicals with  $\text{CH}_4$  molecules. In a dramatic improvement, room temperature transformation of  $\text{CH}_4$  into C1 oxygenates was carried out by Garcia's group under deep (<200 nm) UV illumination in the presence of water and air over the confined space of zeolites' solid surfaces (e.g., beta zeolites) containing hydroxyl functionality (i.e., internal silanol).<sup>[145]</sup> The OH groups on zeolites were cleaved homolytically under deep UV radiation (165 and 185 nm) and generated surface siloxyl (hydroxyl in case of water) radicals in the confined micropores of the zeolites (Figure 11a). In the micropores,  $\bullet\text{OH}$  radicals scavenged the initially formed methyl radicals. As a result,  $\bullet\text{OH}$  radicals were not accessible to large amount of methyl radicals, diminishing the side reactions significantly. Therefore, selectivity toward C1 oxygenate was over 95% at a conversion of 13% within a few minutes. In addition, the authors demonstrated that  $7.16 \text{ Gcal mol}^{-1}$  energy was required

for 13%  $\text{CH}_4$  conversion (185 nm lamp, 1 h irradiation) against  $15.9 \text{ Gcal mol}^{-1}$  energy for  $\text{CH}_4$  transformation to syn gas. However, in the absence of oxygen, low molecular weight alkanes were produced.<sup>[166]</sup> The proposed mechanism for the transformation of  $\text{CH}_4$  using deep UV light over a silica surface is shown in Figure 11a. The selectivity toward methanol was excellent, although hazardous deep UV radiation was used as light source. Two types of UV photoreactors were used for methane conversion as shown in Figure 11b,c.

It is interesting to use laser as light source in photocatalysis because of its high intensity, monochromaticity, and tunability. In this endeavor, Gondal et al. described photocatalytic  $\text{CH}_4$  conversion to generate methanol using a visible laser (argon ion laser, 514 nm) beam over  $\text{WO}_3$ .<sup>[146]</sup> The conversion rate was much faster (within 15 min) compared to the conventional lamps ( $\approx 18$  h) and the products were analyzed to be methanol,  $\text{O}_2$  and  $\text{CO}_2$ . High photon density of laser generated very large concentration of  $\bullet\text{OH}$  radicals, which combined to produce  $\text{H}_2\text{O}_2$  as main source of  $\text{O}_2$ . However, visible laser can show photoactivity only on photocatalysts with bandgap  $\leq 3$  eV. Therefore, the same group investigated UV laser beam (355 nm)-induced photocatalytic  $\text{CH}_4$  conversion over  $\text{WO}_3$ , rutile  $\text{TiO}_2$ , and NiO photocatalysts at room temperature in aqueous suspensions.<sup>[167]</sup> A maximum conversion of  $\approx 29\%$  occurred with  $\text{WO}_3$  photocatalyst for methanol production. In these works,  $\text{CH}_4$  conversion efficiency was not sufficient due to the recombination of the photogenerated charge carriers. This issue was resolved by using  $\text{Ag}^+$  impregnated  $\text{WO}_3$ , wherein the former suppressed the charge recombination rate appreciably to generate higher concentration of  $\bullet\text{OH}$  under a laser beam (100 mJ, 355 nm).<sup>[147]</sup>  $\text{CH}_4$  was converted to methanol with simultaneous formation of hydrogen and oxygen. However, due to the high reactivity of the hydroxyl radicals, several complex side reactions occurred during the photocatalytic process. Moreover, the electron donating nature of methanol limited the yield and selectivity of the product.

Above all,  $\text{WO}_3$ -based photocatalysts are attractive for  $\text{CH}_4$  conversion due to the energy of its valence band maxima ( $E_{\text{VB}} = +3.1 \text{ V vs NHE}$ ), which is suitable for water oxidation to generate hydroxyl radicals successively producing methanol.<sup>[146]</sup> Nanostructured, such as ordered mesoporous,  $\text{WO}_3$  could have enhanced photocatalytic effect due to its porous structure and high specific surface area, which ensure more active sites. In this regard, the work of Villa et al. was noteworthy, who studied the photocatalytic conversion of  $\text{CH}_4$  to methanol in an aqueous suspension over ordered mesoporous  $\text{WO}_3$  exposed to a medium pressure quartz mercury vapor lamp at  $55^\circ\text{C}$ .<sup>[148]</sup> The authors also experimented to understand the effect of the addition of  $\text{H}_2\text{O}_2$  and electron scavengers, such as  $\text{Fe}^{3+}$ ,  $\text{Cu}^{2+}$  and  $\text{Ag}^+$ . Methanol production was improved significantly in the presence of  $\text{Fe}^{3+}$  and  $\text{Cu}^{2+}$  ions, as these species scavenged photogenerated electrons leading to better charge separation. An impressive yield of  $55.5 \mu\text{mol h}^{-1} \text{ g}^{-1}$  was obtained with  $\text{Fe}^{3+}$  ( $2 \times 10^{-3} \text{ M}$ ) incorporated mesoporous  $\text{WO}_3$ . In a contrary, in the presence of  $\text{Ag}^+$  ions, methanol production decreased compared to the pristine mesoporous  $\text{WO}_3$ . The negative effect of  $\text{Ag}^+$  ions was attributed to its reduction and successive deposition of the resulting metallic Ag on  $\text{WO}_3$ . Surface modification of  $\text{WO}_3$  with fluorine decreased the yield of methanol production,<sup>[168]</sup> which could be explained by the generation/presence of excess amount of hydroxyl

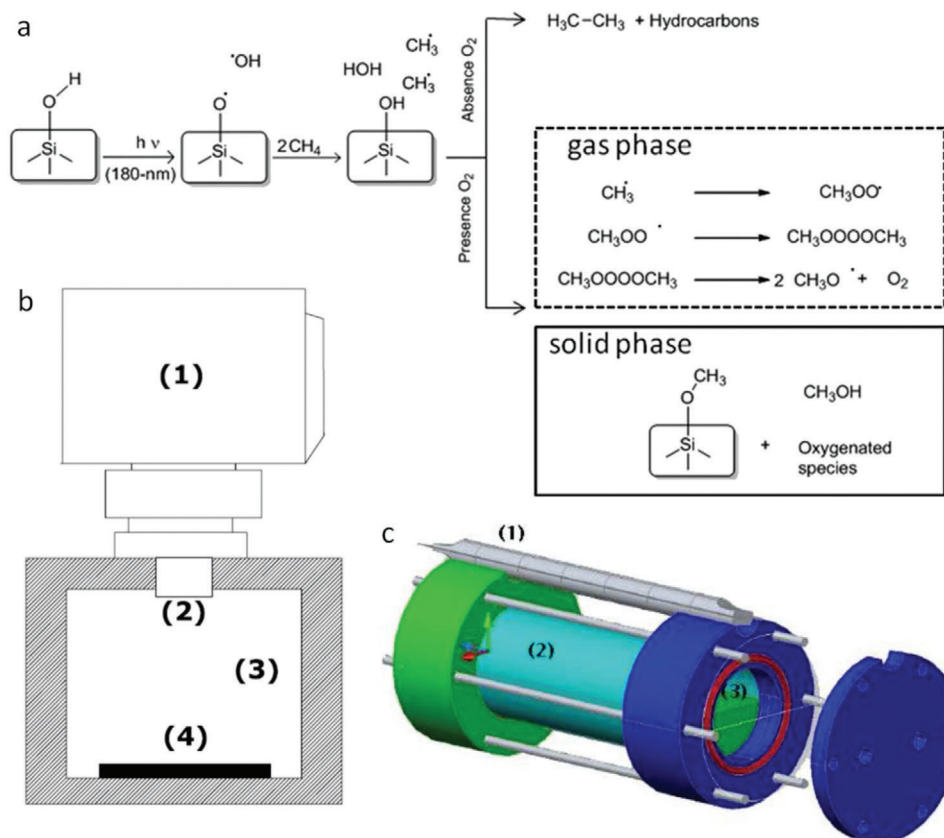


**Figure 11.** a) Schematic representation of  $\text{CH}_4$  oxidation on a silica surface under deep UV light. b) 165 nm photoreactor consisting of 1. deuterium lamp, 2. MgF2 window, 3. gas chamber, and 4. photocatalyst. c) 185 nm photoreactor, 1. Hg lamp, 2. synthetic quartz window, and 3. gas chamber, wherein photocatalyst was placed. Reproduced with permission.<sup>[145]</sup> Copyright 2011, American Chemical Society.

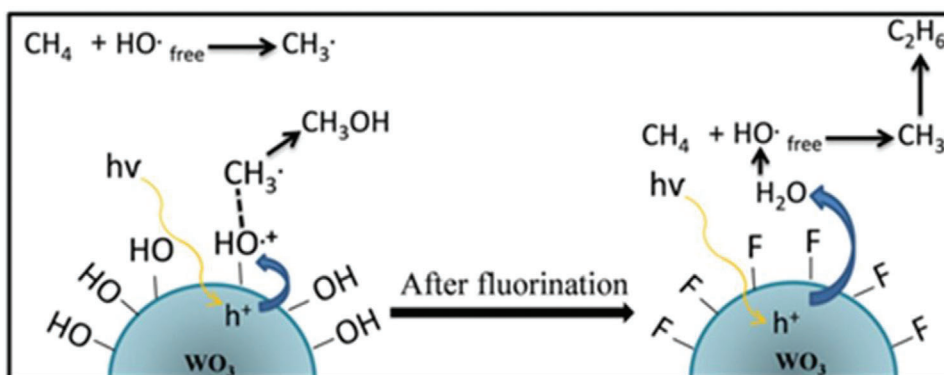


**Figure 12.** Proposed mechanism for selective oxidation of  $\text{CH}_4$  over tungsten oxide and fluorine-modified tungsten oxide. Reproduced with permission.<sup>[168]</sup> Copyright 2014, Elsevier.

radicals that favored the formation of ethane. The mechanism of  $\text{CH}_4$  oxidation on  $\text{WO}_3$  and surface modified  $\text{WO}_3$  with fluorine are shown in **Figure 12**. This issue of lower amount of methanol production was addressed by La doping into mesoporous  $\text{WO}_3$ . A twofold higher product formation rate for methanol compared to pristine  $\text{WO}_3$  was observed, while the  $\text{CO}_2$  generation rate was decreased.<sup>[149]</sup> Considering the importance of developing a photocatalytic system for the direct conversion of  $\text{CH}_4$  to methanol,

only limited efforts have been made in this direction to date. Thus, the advancement of such systems does not meet the demand expected for both academic interests and industrial applications.

Exposed catalyst surface can have significant effect on  $\text{CH}_4$  oxidation activity as well as product selectivity as demonstrated by Zhu et al.<sup>[22]</sup> It was noted that the (102) and (012) facets of bipyramidal  $\text{BiVO}_4$  microcrystals were more active and more selective

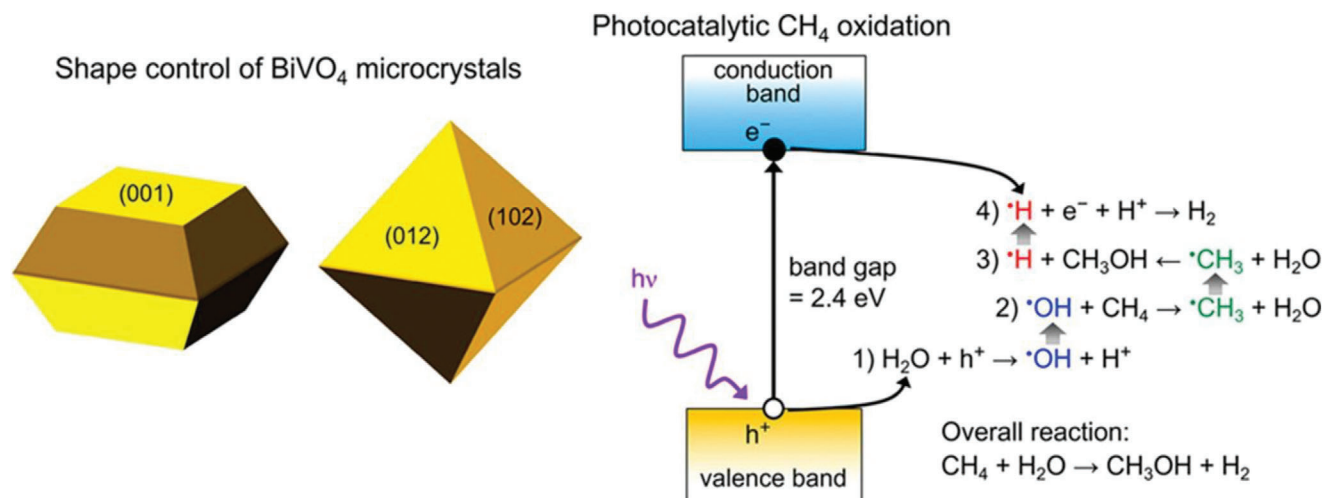


**Figure 13.** Facet-dependent conversion of CH<sub>4</sub> to MeOH over BiVO<sub>4</sub> microcrystals and mechanism of the photocatalysis. Reproduced with permission.<sup>[122]</sup> Copyright 2018, American Chemical Society.

for MeOH production compared to the (001) facets of platelet microcrystals (Figure 13). The highest activity for MeOH production was 151.7 μmol h<sup>-1</sup> g<sup>-1</sup> with > 85% selectivity for 2 h of photocatalysis. The catalytic activity was maintained for >100 μmol h<sup>-1</sup> g<sup>-1</sup> for up to 5 h of photocatalysis. However, thin platelets produced CO<sub>2</sub> as the major product. The valence band-edge of BiVO<sub>4</sub> possesses sufficient energy and the photogenerated holes therein can generate •OH radicals from water oxidation. The successive reactions are shown in Figure 13.

### 3.2.3. Photocatalytic Conversion of CH<sub>4</sub> with CO<sub>2</sub>

In this process, also known as photocatalytic dry reforming of methane (DRM), CO<sub>2</sub> is used to oxidize CH<sub>4</sub>, showing high endothermic nature of the overall chemical reaction ( $\text{CO}_2 + \text{CH}_4 \rightarrow 2\text{CO} + 2\text{H}_2$ ,  $\Delta H_{298\text{K}} = 247 \text{ kJ mol}^{-1}$ ).<sup>[169–171]</sup> The products are not only two important fuels but also vital feedstock for synthesizing valuable chemicals. Moreover, this process minimizes the emission of two greenhouse gases. But CO<sub>2</sub> is more stable (O=C=O, 532 kJ mol<sup>-1</sup> at 298 K) than CH<sub>4</sub> and activation of the C=O bonds is more difficult. Therefore, the conversion of CH<sub>4</sub> and CO<sub>2</sub> to other molecules is thermodynamically unfavorable ( $\Delta G_{298\text{K}} = 170 \text{ kJ mol}^{-1}$ ). Usually, high temperatures are necessary to carry out such conversion. Fortunately, in the presence of photoenergy, a photocatalyst can initiate the process at low temperatures.

In such conversion process, usually CO forms from the reduction of CO<sub>2</sub> by CH<sub>4</sub>.<sup>[150]</sup> Therefore, it is actually reduction of CO<sub>2</sub> rather than oxidation of CH<sub>4</sub>. Nevertheless, Yazdanpour and Sharifnia described the photoconversion of CH<sub>4</sub> and CO<sub>2</sub> over a copper phthalocyanine (CuPc)-modified TiO<sub>2</sub> (CuPc/TiO<sub>2</sub>)-coated stainless steel photocatalyst in a gas phase batch reactor.<sup>[151]</sup> The importance of this work lied in its operation under visible light. Approximately 14% and 18% conversion of, respectively, CO<sub>2</sub> and CH<sub>4</sub> were observed after 240 h. The formed products were different oxygenates, such as CO, aldehyde and ketone. The presence of CuPc shifted the band edge of TiO<sub>2</sub> to the visible region, causing the conversion process to occur under vis-

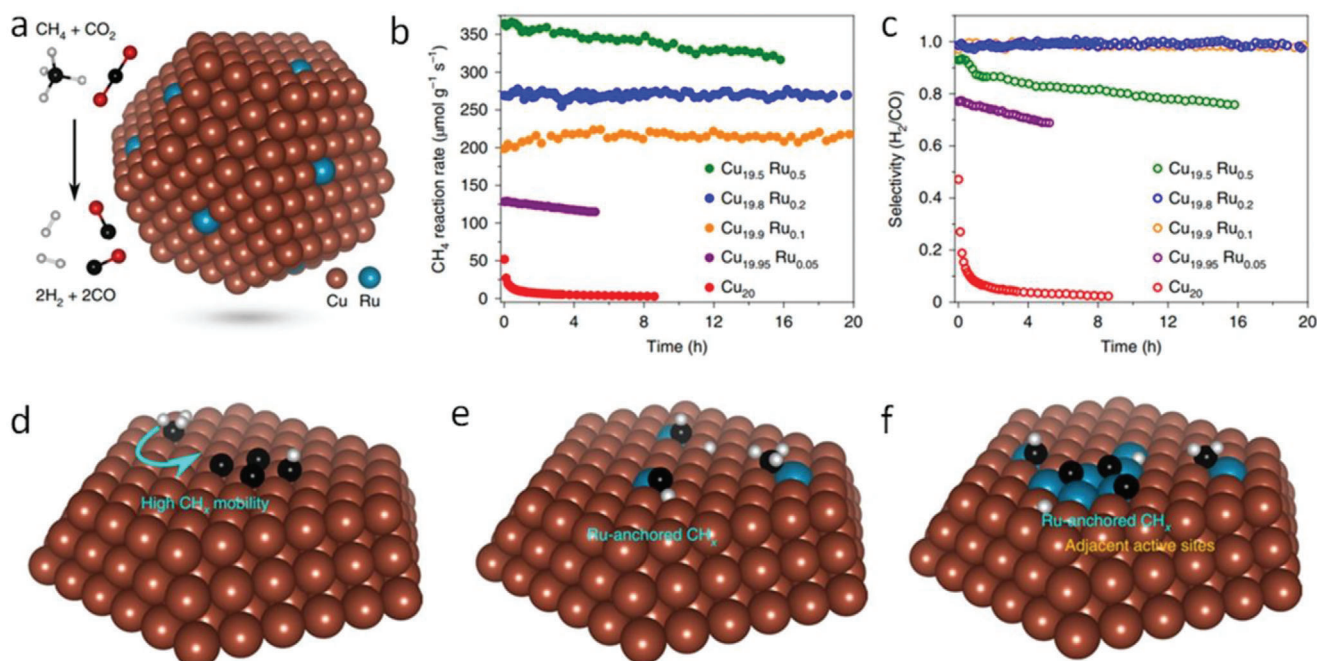
ible light. In order to increase the conversion efficiency, reduction of CO<sub>2</sub> with CH<sub>4</sub> over ZnS/ZnO nanocomposites under UV and visible light was studied. ≈45% and 54% of CO<sub>2</sub> and CH<sub>4</sub> were converted after 5 h of UV light exposure.<sup>[152]</sup>

In a significant progress, Zhou et al. reported photocatalytic DRM over Ru single atoms supported on plasmonic Cu nanoparticles (Figure 14a).<sup>[92]</sup> The plasmonic Cu nanoparticles enabled the alloy to absorb light strongly, while the Ru single atoms increased the catalytic activity. It was noticed that the concentration of Ru single atoms significantly influenced the reaction rate and stability of the catalyst. Pure Cu nanoparticles showed an initial reaction rate of ≈50 μmol CH<sub>4</sub> g<sup>-1</sup> s<sup>-1</sup>, which decreased to ≈4 μmol CH<sub>4</sub> g<sup>-1</sup> s<sup>-1</sup> after ≈5 h (Figure 14b) due to the coke deposition around the catalyst (Figure 14d,f). Addition of extremely low amount of Ru (Cu<sub>19.95</sub>Ru<sub>0.05</sub>) greatly increased the initial reaction rate and stability. Further increase of Ru concentration (Cu<sub>19.9</sub>Ru<sub>0.1</sub> and Cu<sub>19.8</sub>Ru<sub>0.2</sub>) led to achieve stability for 20 h (Figure 14c,e) after which the morphology and the chemical state of the catalyst remained intact. The stability was maintained for 50 h with a minimum loss of catalytic activity for Cu<sub>19.9</sub>Ru<sub>0.1</sub>. At the same time, selectivity (ratio of H<sub>2</sub> to CO production rate) of Cu<sub>19.9</sub>Ru<sub>0.1</sub> and Cu<sub>19.8</sub>Ru<sub>0.2</sub> approached the ideal value 1 (i.e., >99% selectivity). Recently Shoji et al. reported DRM over Rh/SrTiO<sub>3</sub> (STO) under UV light irradiation.<sup>[157]</sup> The Rh nanoparticles acted as the catalytic centers. The catalyst achieved >50% DRM conversion. Although heat was not applied from outside, the catalyst was heated up to 300 °C from the UV irradiation. Notably, in photothermal catalysis the surface temperature can reach 300–500 °C or more and we are not going to discuss it further.<sup>[172]</sup>

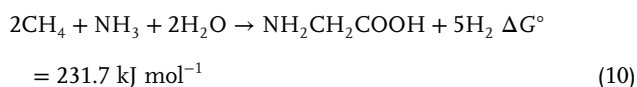
### 3.2.4. Photocatalytic Conversion of CH<sub>4</sub> with NH<sub>3</sub>

As this strategy is not well established and the literature is not rich, we will discuss it briefly. Amino acids and other important molecules were experimentally proved to be produced from a variety of reducing gases, such as CH<sub>4</sub>, H<sub>2</sub>S, and NH<sub>3</sub> using a





range of energy sources, such as UV light, spark discharge, thermal energy, shock waves, and ionizing radiation.<sup>[173–177]</sup> Keeping it in mind, Sagan and Khare reported synthesis of amino acids from a reducing gas mixture of CH<sub>4</sub>, H<sub>2</sub>S, NH<sub>3</sub>, and H<sub>2</sub>O under UV irradiation.<sup>[178]</sup> H<sub>2</sub>S was the long-wavelength photon acceptor for such prebiological organic synthesis. Later, Reiche and Bard reported the production of amino acids by photosynthesis from a mixture of CH<sub>4</sub>, NH<sub>3</sub>, and H<sub>2</sub>O over a Pt/TiO<sub>2</sub> photocatalyst.<sup>[179]</sup> Irradiation of a deaerated aqueous solution of NH<sub>4</sub>Cl (2 M) or NH<sub>3</sub> (≈28%) under continuous and slow CH<sub>4</sub> bubbling in the presence of Pt/TiO<sub>2</sub> (platinized) illuminated by a xenon lamp (2.5 kW operated at 1.6 kW) produced a mixture of amino acids after 64–66 h. ≈0.5 and 0.2 μmol amino acids were produced in an NH<sub>4</sub>Cl and NH<sub>3</sub> solution, respectively. The amino acids glycine, alanine, serine, aspartic acid, and glutamic acid were generated. This result demonstrated the photosynthesis of amino acids in a heterogeneous system under irradiation by near-UV-visible light. The photosynthesis reaction did not occur on the pure TiO<sub>2</sub> surface due to the lack of reduction sites. The overall reaction was as follows



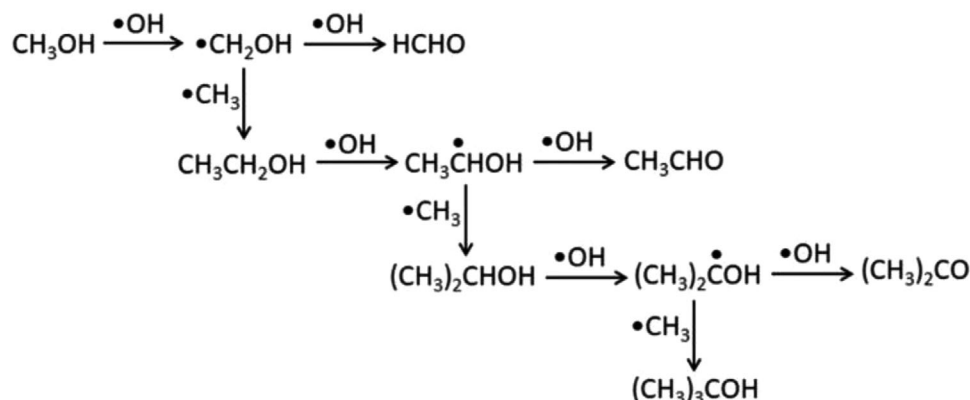
Mechanism studies by Bard and co-workers revealed the involvement of hydroxyl radicals in the photosynthesis process.<sup>[180]</sup> In addition to the amino acids, methanol, and ethanol were also produced. However, further research in this field is missing in the literature.

### 3.3. Photoelectric Conversion of CH<sub>4</sub>

Combining photocatalysis and electrocatalysis resulting in photoelectrode (photoelectric or photoelectrochemical (PEC) technique) is an interesting technique that can provide additional energy to meet the energy demand for breaking the inert C–H bonds in CH<sub>4</sub>. In this technique, methane oxidation occurs at the interface of the photoanode and electrolyte by the action of both irradiated light and applied potential. Photoelectrocatalyst can play important role to oxidize methane to oxygenates selectively at low temperatures as it has the advantage of monitoring the applied potential. We are not going to discuss it in details as it was covered in other review at length.<sup>[93]</sup>

### 3.4. Photochemical Processes for CH<sub>4</sub> Activation

Activation of the C–H bonds in CH<sub>4</sub> only by light, especially deep UV radiation is another approach for CH<sub>4</sub> oxidation. This section is devoted exclusively to photochemical conversion, i.e., conversion carried out by photoroutes and chemical routes. Photochemical conversion is very convenient and economical because it requires only light. Although thus far the least explored of the categories, photochemical processes could be a promising alternative for the conversion of relatively inert CH<sub>4</sub> to oxygenates under mild conditions without using a catalyst. Initial attempts were made in Japan at Yamaguchi University, where Ogura and Kataoka developed oxidative conversion of CH<sub>4</sub> to alcohols, acids and ketones by a photochemical reaction with water vapor at atmospheric pressure and temperatures below 100 °C.<sup>[76]</sup> To carry



**Scheme 2.** A generalized scheme to obtain different products according to Ogura and Kataoka. Reproduced with permission.<sup>[76]</sup> Copyright 1988, Elsevier.

out such oxidation, CH<sub>4</sub> and water vapor were fed into a reaction chamber. The gas mixture was exposed to a 20 W low pressure mercury lamp with illumination wavelengths of 185 and 254 nm. The water underwent dissociation by UV light according to the following reactions



Successively, each hydroxyl radical abstracted a hydrogen atom from CH<sub>4</sub> to initiate its conversion and generated a methyl radical, which then reacted with a water molecule to give methanol as shown below



Methanol was the major product, with a selectivity of  $\approx 70\%$  at 90 °C. Higher species, such as formic acid, ethanol, formaldehyde, acetone, and acetic acid were formed with selectivity of 11%, 5%, 5%, 4%, and 3%, respectively, which were possibly originated from methanol. Notably, no higher alkanes were formed and the coupling of methyl radicals was insignificant. Large amounts of acetic acid and formic acid were formed with the addition of oxygen gas to the reaction mixture. A generalized reaction pathway for the generation of different products is depicted in **Scheme 2**. A similar work described oxidative CH<sub>4</sub> conversion by photolysis in the presence of water vapor and air at 100 °C and atmospheric pressure.<sup>[181]</sup> Methane conversion occurred in the range of 4–16%, with selectivity for methanol was over 33%.

### 3.5. Photocatalytic Oxidation of CH<sub>4</sub> with H<sub>2</sub>O<sub>2</sub>

Hydrogen peroxide is a strong and green oxidizing agent that was usually used for partial oxidation of CH<sub>4</sub> in thermocatalysis. However, it can be used for photocatalytic oxidation of CH<sub>4</sub>. Methane activation usually proceeds with the formation of  $\bullet\text{CH}_3$  radicals that often undergo various reactions. This is

the main reason for poor product selectivity in methane oxidation. Nonetheless, Yang et al. engineered mesoporous WO<sub>3</sub> (m-WO<sub>3</sub>) with amorphous FeOOH (FeOOH/m-WO<sub>3</sub>) and reported photocatalytic partial oxidation of methane in the presence of H<sub>2</sub>O<sub>2</sub>.<sup>[155]</sup> The CH<sub>4</sub> conversion rate and product selectivity depended on the composition of the catalyst and the amount of H<sub>2</sub>O<sub>2</sub> used. The catalyst 1.98% FeOOH/m-WO<sub>3</sub> exhibited the highest methane conversion rate (4.68% and 238.6  $\mu\text{mol g}^{-1} \text{h}^{-1}$ ) as well as methanol production rate (211.2  $\mu\text{mol g}^{-1} \text{h}^{-1}$ ) (**Figure 15a**). **Figure 15b** shows that with the increasing concentration of H<sub>2</sub>O<sub>2</sub> methane conversion rate increased. However, methanol production rate reached a maximum when the concentration of H<sub>2</sub>O<sub>2</sub> was 1.5 mmol. More concentration of H<sub>2</sub>O<sub>2</sub> led to decreased MeOH production rate and increased CO<sub>2</sub> amount. The optimized catalyst achieved 91.0% selectivity for methanol production. The catalyst displayed considerable stability for up to six cycles (**Figure 15c**). Methane conversion rate decreased slightly from 238.6 to 223.7  $\mu\text{mol g}^{-1} \text{h}^{-1}$  in the sixth cycle. MeOH production rate decreased from 211.2  $\mu\text{mol g}^{-1} \text{h}^{-1}$  in the first cycle to 191.8  $\mu\text{mol g}^{-1} \text{h}^{-1}$  in the sixth cycle. The observed decrease in methane conversion rate and methanol production rate was due to the slight decrease in Fe content after sixth cycle (1.19 wt% against 1.25 wt% for the fresh catalyst) as evidenced by inductively coupled plasma atomic emission spectroscopic (ICP–AES) data. Moreover, XPS did not show any obvious change in the chemical state of the fresh and the used catalyst. In a proposed mechanism, methane was activated to  $\bullet\text{CH}_3$  radicals by the photo-generated holes at the valence band of m-WO<sub>3</sub>, while  $\bullet\text{OH}$  radicals were generated by the decomposition of H<sub>2</sub>O<sub>2</sub> by the photoelectrons of FeOOH. These radicals then combined to produce methanol selectively. On the other hand, Xie et al. reported FeO<sub>x</sub> anchored TiO<sub>2</sub> photocatalyst for selective oxidation of CH<sub>4</sub> to MeOH in the presence of H<sub>2</sub>O<sub>2</sub> at room temperature and atmospheric pressure.<sup>[158]</sup> The authors studied several metal oxides and noble metals and established that it was the iron oxide that was the most active for this transformation. A CH<sub>4</sub> conversion rate of 15% was reported. Results on different metal oxide loaded on TiO<sub>2</sub> showed that a maximum methanol production was achieved on FeO<sub>x</sub> loaded TiO<sub>2</sub> (**Figure 15d,e**). A maximum yield for methanol production of 1056  $\mu\text{mol g}^{-1}$  of catalyst was obtained on 0.33 wt% FeO<sub>x</sub>/TiO<sub>2</sub>. Notably, in this work the authors achieved high selectivity for alcohol (> 97%), wherein the

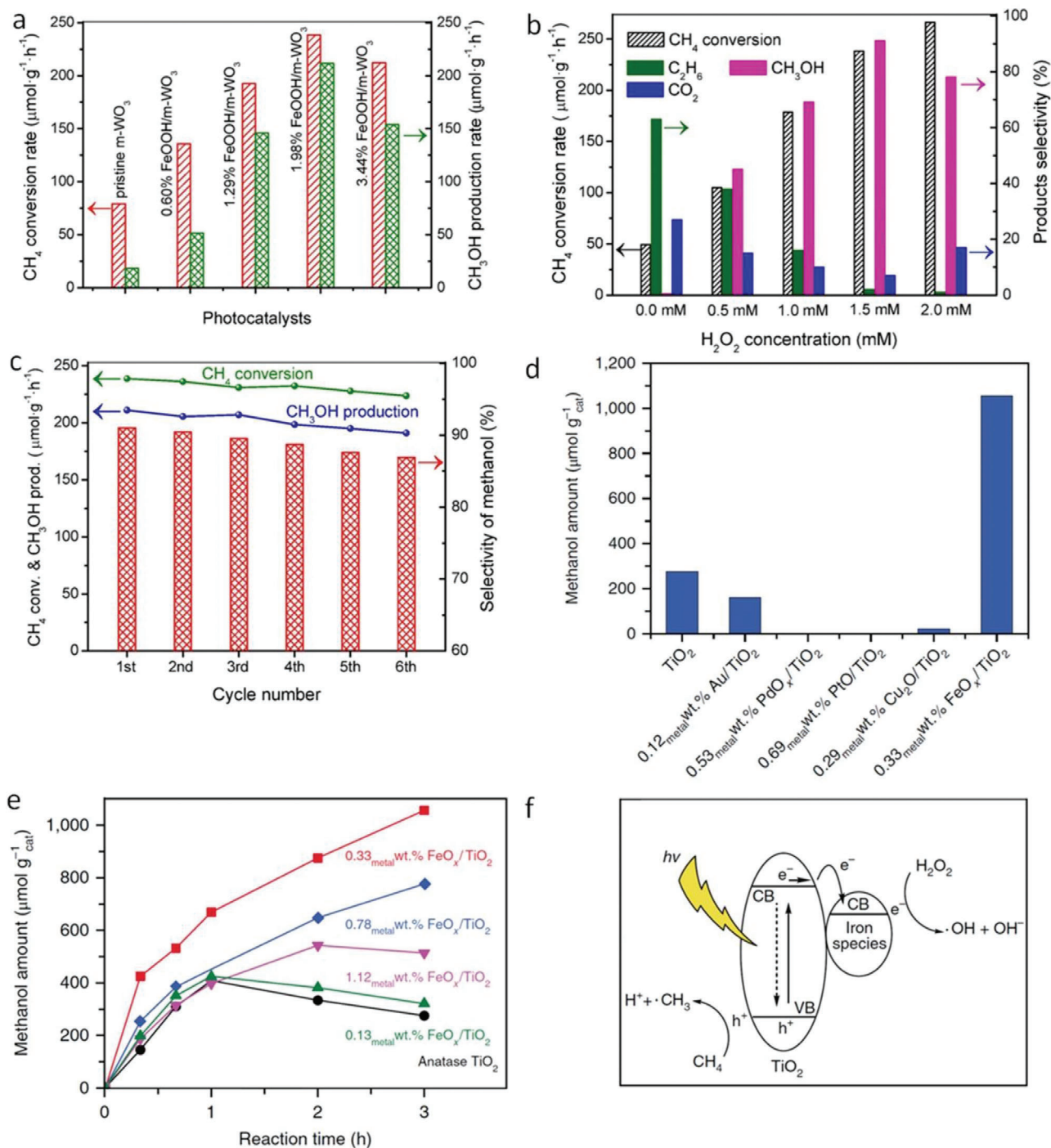


**Figure 15.** a) CH<sub>4</sub> conversion rate and methanol production rate over different catalysts, b) methane conversion rate, and product selectivity over 1.98% FeOOH/m-WO<sub>3</sub> as the concentration of H<sub>2</sub>O<sub>2</sub> varied. c) Methane conversion, methanol production, and selectivity over 1.98% FeOOH/m-WO<sub>3</sub> in different cycles. Reproduced with permission.<sup>[155]</sup> Copyright 2020, Elsevier. d) Methanol production over different catalysts and e) over different amount of FeO<sub>x</sub>-loaded TiO<sub>2</sub>. f) Photocatalytic mechanism. Reproduced with permission.<sup>[158]</sup> Copyright 2018, the authors, published by Springer Nature Limited.

selectivity for methanol generation was >90% with the optimized catalyst. The optimized photocatalyst showed good stability for three runs without any loss of catalytic activity. Proposed mechanism for photocatalytic methane oxidation to methanol is shown in Figure 15f.

### 3.6. Other Processes for CH<sub>4</sub> Oxidation

Electric fields can be used to influence catalytic activity and selectivity of chemical reactions involving polarizable system, such as MeOH and metal/metal oxide support.<sup>[182]</sup> External electric

field can influence the adsorption energies of adsorbates on catalyst surface by changing the internal electric field of the catalyst (support) and adsorbates. Recently, through DFT calculations, Yeh et al. demonstrated that a positive electric field enhanced the oxidation of  $\text{CH}_4$  to  $\text{HCHO}$  by  $\text{O}_2$  over the oxygen-rich (110) surface of  $\text{IrO}_2$ .<sup>[183]</sup> External electric field can suppress methane reforming temperature considerably.<sup>[184]</sup> In addition, plasma can oxidize methane as can be seen in the following review.<sup>[185]</sup> Nevertheless, Wang et al. described plasma assisted synthesis of oxygenates from  $\text{CH}_4$  and  $\text{CO}_2$  in one step at 30 °C and atmospheric pressure.<sup>[186]</sup> The total selectivity to oxygenates ( $\text{CH}_3\text{COOH}$ ,  $\text{MeOH}$ ,  $\text{EtOH}$ , and  $\text{HCHO}$ ) was 59.1% in which the major product was  $\text{CH}_3\text{COOH}$  for which the selectivity was 33.7%. Notably the combination of plasma with the catalyst  $\text{Cu}/\gamma\text{-Al}_2\text{O}_3$  increased acetic acid selectivity to 40.2%.

#### 4. Conclusions and Future Perspectives

In order to build a better future and to cope with the environmental issues, we need to look for alternative energy sources other than the traditional fossil fuel, which releases considerable amount of  $\text{CO}_2$  and causes global warming. In this endeavor, we can turn our attention to  $\text{CH}_4$ , the main constituent of natural gas that supplies  $\approx 21\%$  of world's energy demand. On combustion,  $\text{CH}_4$  releases a large amount of energy with minimum emission of  $\text{CO}_2$ . Activation of  $\text{CH}_4$  is of remarkable importance, because this process will warrant future supplies of energy and fuel. It is also highly desirable for the synthesis of fine chemicals and pharmaceutical products. Unfortunately, the activation process faces kinetic limitations that lead to the formation of  $\text{CO}_2$  or poor product yields. Significant research effort has been made thus far for  $\text{CH}_4$  oxidation. However, efficient and well-controlled  $\text{CH}_4$  oxidation process under mild conditions remains challenging. Many results are at an early stage and far from industrial applications due to the low conversion efficiency, slow rate of reactions and lack of economic competitiveness. Improvement of these techniques is expected to significantly ameliorate global environmental issues, as well as offer alternative energy sources. Fortunately, all these studies have led to progress in the fundamental knowledge of  $\text{CH}_4$  oxidation, catalyst design, syntheses, in situ and ex situ characterization and theoretical studies. Nevertheless, it is important to design more efficient catalysts that offer efficient conversion and desired selectivity for  $\text{CH}_4$  conversion. In the following paragraphs, we demonstrate a few research directions for  $\text{CH}_4$  oxidation that researchers might like to especially engage in to realize significant progress in future.

Electrochemical techniques are fascinating for the  $\text{CH}_4$  oxidation at low temperatures to produce value-added chemicals. However, here main issue is the low solubility of  $\text{CH}_4$  in aqueous solution at standard conditions. This challenge can be overcome by adopting the following approaches. i) We can employ GDEs in the electrolyte.  $\text{CH}_4$  gas can be introduced into the active site of the electrolyte through a gas diffusion layer in the GDEs. The continuous supply of  $\text{CH}_4$  into the GDEs is expected to increase  $\text{CH}_4$  oxidation current that may fulfill the requirements for industrial applications, over the conventional submerged electrodes. ii) The solubility of  $\text{CH}_4$  could also be increased by increasing the pressure and decreasing the temperature of the electrolyte. iii) Using appropriate organic solvents could be an interesting alternative

to circumvent the low solubility problem of  $\text{CH}_4$  in water. Organic solvents may lead to the formation of different products than those obtained in aqueous electrolytes. Additionally, organic solvents are less susceptible to undergo electrocatalytic oxidation unlike water. Thus, the issue of water oxidation (oxygen evolution that may damage the electrocatalyst by oxidation) could be avoided by using aprotic organic solvents. In fact, this area of research was not paid much attention so far and is awaiting further exploration.

Looking for electrocatalytic  $\text{CH}_4$  oxidation processes that lead  $\text{C}_2/2+$  products is another important direction, which must be considered by researcher, because it will add more value to the oxidation. Low electrical conductivity of the electrocatalysts is another challenge that increases charge transfer resistance at the interface. It can be greatly improved by designing composites with carbon-based materials. Doping foreign elements into the active electrocatalysts not only alters the electronic properties of the latter but also enhances their electrical conductivity that improves catalytic activity. Another important aspect of electrocatalytic  $\text{CH}_4$  oxidation is the identification of the rate determining step (RDS) for the development of electrocatalysts. Charge transfer mechanism investigation will help to identify the RDS and overall, the development of electrocatalyst. In this regard, in situ and in operando spectroscopy and other in situ characterizations (such as, TEM, X-ray diffraction, infra-red spectroscopy) along with DFT calculations should be intensively performed to understand and engineer the existing electrocatalysts and discover new ones.

Photocatalysis is another promising technology for  $\text{CH}_4$  oxidation at low temperatures. The most important part of such research is to develop an efficient photocatalyst that can absorb light (preferably visible) efficiently and generate charge carriers owning sufficient energy to drive  $\text{CH}_4$  oxidation. This issue can be solved by designing a composite catalyst system, as a single photocatalyst often cannot satisfy all these conditions. A possible way out is to design a Z-scheme photocatalyst system that has stronger ability to drive a photocatalytic reaction, unlike a conventional type II heterojunction. In many photocatalytic  $\text{CH}_4$  oxidation processes, hydroxyl radicals are the main intermediates. Unfortunately, due to the high reactivity of hydroxyl radicals, selectivity is often compromised. Controlled release of hydroxyl radicals could be a possible solution. Another important research direction is to employ PEC devices for  $\text{CH}_4$  oxidation to valuable organic compounds as demonstrated by Jin in a recent editorial.<sup>[187]</sup> Recently, Grätzel and co-workers. used PEC cell to synthesize high-value added organics from arene C–H amination.<sup>[188]</sup> In addition,  $\text{H}_2\text{O}_2$  production by PEC recently attracted much interest.<sup>[189]</sup> Such in situ generated  $\text{H}_2\text{O}_2$  could be used for  $\text{CH}_4$  oxidation. These proposition and experimental evidence indicate prospects of PEC devices for  $\text{CH}_4$  activation where researchers are strongly recommended to pay attention. Considering these factors may lead to a photocatalyst or PEC system design that can oxidize  $\text{CH}_4$  proficiently for durable and practical applications in industry. Moreover, looking for highly active, stable and more selective catalysts is urgently necessary to make the  $\text{CH}_4$  activation process more economical.

Another research direction we would like to emphasize particularly is to use metal–organic framework (MOF) for both

electrocatalytic and photocatalytic oxidation of CH<sub>4</sub>. The intrinsic characteristics of MOF would enable adsorption of large amount of CH<sub>4</sub> onto the catalyst surface. Moreover, the organic moiety of MOF may be favorable for CH<sub>4</sub> adsorption. Therefore, it would be interesting to see the catalytic properties of MOF for CH<sub>4</sub> oxidation. Developing composite catalysts with MOFs and other catalysts may be a good proposition to improve catalytic efficiency. Nanocomposites of metal single atoms on porous carbon-based supports can be used for photocatalyst and electrocatalyst for CH<sub>4</sub> oxidation. The ultimate goal is to design high efficient, highly selective, durable, and cost-effective photocatalysts and electrocatalysts for CH<sub>4</sub> oxidation.

Long-term stability and durability of the catalyst and selectivity of product are two critical issues for methane oxidation in both electrocatalysis and photocatalysis. Engineering the interface of a heterostructure can improve long-term stability and durability of a catalyst by minimizing the agglomeration of the particles. Such engineering also may be able to minimize the coking on the catalyst surface. In this regard, very low concentration or single atoms of the active catalyst over the support is interesting. On the other hand, thorough understanding of the mechanism of a catalytic process by theoretical and experimental studies will enable us to improve selectivity of a desired product. Controlling the pressure of CH<sub>4</sub> on the catalyst surface can improve selectivity. In this regard, a GDE can be used. Proper electrochemical cell design, electrolyte, reaction conditions, such as temperature, pressure, etc. and the choice of oxidizing agents also play important role in product selectivity.

Finally, technical and economic analyses that include cost of device manufacturing, carbon and energy efficiencies and product purification and distribution costs for methane oxidation via electrocatalytic and photocatalytic process needs to be considered. Computer-based simulations are necessary to assess the performance of each process for a desired product. Very recently, Alsuhaibani et al. demonstrated that the reduction in reaction pressure of the reactor that produced methanol from shale gas resulted in substantial improvement of the profit of a plant with capacity of  $2.1 \times 10^6$  tons per year.<sup>[190]</sup> Therefore, we can conclude that, from techno-economic view point, methane oxidation to a desired product by electrocatalysis and photocatalysis in industrial scale is expected to be economically viable.

## Acknowledgements

J.H.P. acknowledges the financial support by the NRF research grant (2019R1A2C3010479, 2019M1A2A2065612, 2019M3E6A1064525, 2019R1A4A1029237). M.M. acknowledges the financial support by the National Natural Science Foundation of China (21905298).

## Conflict of Interest

The authors declare no conflict of interest.

## Keywords

electrocatalysis, methane oxidation, oxygenates, photocatalysis, product selectivity and low temperatures, stability

Received: May 25, 2020  
Revised: August 22, 2020  
Published online: October 27, 2020

- [1] H. Peng, C. Rao, N. Zhang, X. Wang, W. Liu, W. Mao, L. Han, P. Zhang, S. Dai, *Angew. Chem., Int. Ed.* **2018**, *57*, 8953.
- [2] W. S. Reeburgh, *Chem. Rev.* **2007**, *107*, 486.
- [3] D. Saha, H. A. Grappe, A. Chakraborty, G. Orkoulas, *Chem. Rev.* **2016**, *116*, 11436.
- [4] P. Tang, Q. Zhu, Z. Wu, D. Ma, *Energy Environ. Sci.* **2014**, *7*, 2580.
- [5] A. Caballero, P. J. Pérez, *Chem. Soc. Rev.* **2013**, *42*, 8809.
- [6] M. Ravi, M. Ranocchiaro, J. A. van Bokhoven, *Angew. Chem., Int. Ed.* **2017**, *56*, 16464.
- [7] J. Le Mer, P. Roger, *Eur. J. Soil Biol.* **2001**, *37*, 25.
- [8] R. Grilli, J. Triest, J. Chappellaz, M. Calzas, T. Desbois, P. Jansson, C. Guillermin, B. Ferré, L. Lechevallier, V. Ledoux, D. Romanini, *Environ. Sci. Technol.* **2018**, *52*, 10543.
- [9] B. S. Liu, L. Tian, L. Li, C. T. Au, A. S.-C. Cheung, *AIChE J.* **2011**, *57*, 1852.
- [10] Z. R. Chong, S. H. B. Yang, P. Babu, P. Linga, X. Sen Li, *Appl. Energy* **2016**, *162*, 1633.
- [11] B. Buffett, D. Archer, *Earth Planet. Sci. Lett.* **2004**, *227*, 185.
- [12] Z. Yin, P. Linga, *Chin. J. Chem. Eng.* **2019**, *27*, 2026.
- [13] B. Wang, S. Albarracín-Suazo, Y. Pagán-Torres, E. Nikolla, *Catal. Today* **2017**, *285*, 147.
- [14] M. Danielis, S. Colussi, C. de Leitenburg, L. Soler, J. Llorca, A. Trovarelli, *Angew. Chem., Int. Ed.* **2018**, *57*, 10212.
- [15] J. N. Jocz, A. J. Medford, C. Sievers, *ChemCatChem* **2019**, *11*, 593.
- [16] A. Galadima, O. Muraza, *J. Ind. Eng. Chem.* **2016**, *37*, 1.
- [17] I. Y. Hwang, S. H. Lee, Y. S. Choi, S. J. Park, J. G. Na, I. S. Chang, C. Kim, H. C. Kim, Y. H. Kim, J. W. Lee, E. Y. Lee, *J. Microbiol. Biotechnol.* **2014**, *24*, 1597.
- [18] R. K. Thauer, *Angew. Chem., Int. Ed.* **2010**, *49*, 6712.
- [19] S. Jeong, X. Cui, D. R. Blake, B. Miller, S. A. Montzka, A. Andrews, A. Guha, P. Martien, R. P. Bambha, B. LaFranchi, H. A. Michelsen, C. B. Clements, P. Glaize, M. L. Fischer, *Geophys. Res. Lett.* **2017**, *44*, 486.
- [20] H. Blanco, W. Nijs, J. Ruf, A. Faaij, *Appl. Energy* **2018**, *232*, 323.
- [21] L. Yuliaty, H. Yoshida, *Chem. Soc. Rev.* **2008**, *37*, 1592.
- [22] W. Zhu, M. Shen, G. Fan, A. Yang, J. R. Meyer, Y. Ou, B. Yin, J. Fortner, M. Foston, Z. Li, Z. Zou, B. Sadtler, *ACS Appl. Nano Mater.* **2018**, *1*, 6683.
- [23] M. J. McAnulty, V. G. Poosarla, K. Y. Kim, R. Jasso-Chávez, B. E. Logan, T. K. Wood, *Nat. Commun.* **2017**, *8*, 15419.
- [24] A. V. Milkov, *Earth-Sci. Rev.* **2004**, *66*, 183.
- [25] A. I. Olivos-Suarez, Á. Szécsényi, E. J. M. Hensen, J. Ruiz-Martinez, E. A. Pidko, J. Gascon, *ACS Catal.* **2016**, *6*, 2965.
- [26] G. Li, W. Hu, F. Huang, J. Chen, M. C. Gong, S. Yuan, Y. Chen, L. Zhong, *Can. J. Chem. Eng.* **2017**, *95*, 1117.
- [27] R. Abbasi, G. Huang, G. M. Istratescu, L. Wu, R. E. Hayes, *Can. J. Chem. Eng.* **2015**, *93*, 1474.
- [28] Y. Dai, V. P. Kumar, C. Zhu, H. Wang, K. J. Smith, M. O. Wolf, M. J. MacLachlan, *Adv. Funct. Mater.* **2019**, *29*, 1807519.
- [29] K. Wu, L.-D. Sun, C.-H. Yan, *Adv. Energy Mater.* **2016**, *6*, 1600501.
- [30] M. Etminan, G. Myhre, E. J. Highwood, K. P. Shine, *Geophys. Res. Lett.* **2016**, *43*, 12614.
- [31] J. G. Vitillo, A. Bhan, C. J. Cramer, C. C. Lu, L. Gagliardi, *ACS Catal.* **2019**, *9*, 2870.
- [32] L. Arnarson, P. S. Schmidt, M. Pandey, A. Bagger, K. S. Thygesen, I. E. L. Stephens, J. Rossmeisl, *Phys. Chem. Chem. Phys.* **2018**, *20*, 11152.

- [33] J. Baek, B. Rungtaweeworani, X. Pei, M. Park, S. C. Fakra, Y.-S. Liu, R. Matheu, S. A. Alshmiri, S. Alshehri, C. A. Trickett, G. A. Somorjai, O. M. Yaghi, *J. Am. Chem. Soc.* **2018**, *140*, 18208.
- [34] H. Schwarz, *Angew. Chem., Int. Ed.* **2011**, *50*, 10096.
- [35] N. Agarwal, S. J. Freakley, R. U. Mcvicker, S. M. Althahban, N. Dimitratos, Q. He, D. J. Morgan, R. L. Jenkins, D. J. Willock, S. H. Taylor, C. J. Kiely, G. J. Hutchings, *Science* **2017**, *358*, 223.
- [36] B. Christian Enger, R. Lødeng, A. Holmen, *Appl. Catal., A* **2008**, *346*, 1.
- [37] Y. H. Hu, E. Ruckenstein, *Adv. Catal.* **2004**, *48*, 297.
- [38] L. Yang, H. Huang, *Chem. Rev.* **2015**, *115*, 3468.
- [39] D. Balcells, E. Clot, O. Eisenstein, *Chem. Rev.* **2010**, *110*, 749.
- [40] P. Schwach, X. Pan, X. Bao, *Chem. Rev.* **2017**, *117*, 8497.
- [41] W. G. Cui, G. Y. Zhang, T. L. Hu, X. H. Bu, *Coord. Chem. Rev.* **2019**, *387*, 79.
- [42] Z. Li, G. B. Hoflund, *J. Nat. Gas Chem.* **2003**, *12*, 153.
- [43] S. L. Caldwell, J. R. Laidler, E. A. Brewer, J. O. Eberly, S. C. Sandborgh, F. S. Colwell, *Environ. Sci. Technol.* **2008**, *42*, 6791.
- [44] N. J. Gunsalus, A. Koppaka, S. H. Park, S. M. Bischof, B. G. Hashiguchi, R. A. Periana, *Chem. Rev.* **2017**, *117*, 8521.
- [45] W. Wang, C. Su, Y. Wu, R. Ran, Z. Shao, *Chem. Rev.* **2013**, *113*, 8104.
- [46] X. Meng, X. Cui, N. P. Rajan, L. Yu, D. Deng, X. Bao, *Chem* **2019**, *5*, 2296.
- [47] C. Li, W. Yan, Q. Xin, *Catal. Lett.* **1994**, *24*, 249.
- [48] M. S. A. Sher Shah, J. Lee, A. Rauf, J. H. Park, B. Lim, P. J. Yoo, *Nanoscale* **2018**, *10*, 19498.
- [49] E. Broctawik, *Adv. Quantum Chem.* **1998**, *33*, 349.
- [50] J. E. Collin, J. Delwiche, *Can. J. Chem.* **1967**, *45*, 1875.
- [51] N. D. Epiotis, *J. Mol. Struct.: THEOCHEM* **1988**, *169*, 289.
- [52] P. L. Arnold, M. W. McMullon, J. Rieb, F. E. Kühn, *Angew. Chem., Int. Ed.* **2015**, *54*, 82.
- [53] B. G. Hashiguchi, S. M. Bischof, M. M. Konnick, R. A. Periana, *Acc. Chem. Res.* **2012**, *45*, 885.
- [54] G. Li, M. Qian, J. Kang, S. Liu, C. Ren, J. Zhang, D. Wang, *Jpn. J. Appl. Phys.* **2018**, *57*, 096204.
- [55] J. Xu, R. D. Armstrong, G. Shaw, N. F. Dummer, S. J. Freakley, S. H. Taylor, G. J. Hutchings, *Catal. Today* **2016**, *270*, 93.
- [56] C. G. Zhan, J. A. Nichols, D. A. Dixon, *J. Phys. Chem. A* **2003**, *107*, 4184.
- [57] J. Berkowitz, J. P. Greene, H. Cho, B. Ruscić, *J. Chem. Phys.* **1987**, *86*, 674.
- [58] A. Komornicki, D. A. Dixon, *J. Chem. Phys.* **1992**, *97*, 1087.
- [59] M. C. Paganini, M. Chiesa, P. Martino, E. Giamello, E. Garrone, *J. Phys. Chem. B* **2003**, *107*, 2575.
- [60] R. Horn, R. Schlögl, *Catal. Lett.* **2015**, *145*, 23.
- [61] P. Tomkins, M. Ranocchiari, J. A. Van Bokhoven, *Acc. Chem. Res.* **2017**, *50*, 418.
- [62] M. J. Brown, N. D. Parkyn, *Catal. Today* **1991**, *8*, 305.
- [63] A. A. Latimer, A. Kakekhani, A. R. Kulkarni, J. K. Nørskov, *ACS Catal.* **2018**, *8*, 6894.
- [64] J. A. Labinger, *J. Mol. Catal. A: Chem.* **2004**, *220*, 27.
- [65] M. He, J. Zhang, X.-L. Sun, B.-H. Chen, Y.-G. Wang, *J. Phys. Chem. C* **2016**, *120*, 27422.
- [66] F. Thalasso, A. Vallecillo, P. García-Encina, F. Fdz-Polanco, *Water Res.* **1997**, *31*, 55.
- [67] O. Modin, K. Fukushi, K. Yamamoto, *Water Res.* **2007**, *41*, 2726.
- [68] D. Bastviken, J. Ejelrtsson, I. Sundh, L. J. Tranvik, *Ecology* **2003**, *84*, 969.
- [69] X. Zang, W. Chen, X. Zou, J. N. Hohman, L. Yang, B. Li, M. Wei, C. Zhu, J. Liang, M. Sanghadasa, J. Gu, L. Lin, *Adv. Mater.* **2018**, *30*, 1805188.
- [70] J. Kibsgaard, T. F. Jaramillo, *Angew. Chem., Int. Ed.* **2014**, *53*, 14433.
- [71] B. Liu, Y.-F. Zhao, H.-Q. Peng, Z.-Y. Zhang, C.-K. Sit, M.-F. Yuen, T.-R. Zhang, C.-S. Lee, W.-J. Zhang, *Adv. Mater.* **2017**, *29*, 1606521.
- [72] A. Iulianelli, S. Liguori, J. Wilcox, A. Basile, *Catal. Rev.: Sci. Eng.* **2016**, *58*, 1.
- [73] G. Kreysa, K. Jüttner, *Angew. Chem., Int. Ed.* **2008**, *47*, 5881.
- [74] N. Spinner, W. E. Mustain, *J. Electrochem. Soc.* **2013**, *160*, F1275.
- [75] L. Yuliyati, H. Itoh, H. Yoshida, *Chem. Phys. Lett.* **2008**, *452*, 178.
- [76] K. Ogura, M. Kataoka, *J. Mol. Catal.* **1988**, *43*, 371.
- [77] R. Balasubramanian, S. M. Smith, S. Rawat, L. A. Yatsunyk, T. L. Stemmler, A. C. Rosenzweig, *Nature* **2010**, *465*, 115.
- [78] F. E. Zilly, J. P. Acevedo, W. Augustyniak, A. Deege, M. T. Reetz, *Angew. Chem., Int. Ed.* **2011**, *50*, 2720.
- [79] M. Merx, D. A. Kopp, M. H. Sazinsky, J. L. Blazyk, J. Müller, S. J. Lippard, *Angew. Chem., Int. Ed.* **2001**, *40*, 2782.
- [80] H. Arakawa, M. Aresta, J. N. Armor, M. A. Barteau, E. J. Beckman, A. T. Bell, J. E. Bercaw, C. Creutz, E. Dinjus, D. A. Dixon, K. Domen, D. L. DuBois, J. Eckert, E. Fujita, D. H. Gibson, W. A. Goddard, D. W. Goodman, J. Keller, G. J. Kubas, H. H. Kung, J. E. Lyons, L. E. Manzer, T. J. Marks, K. Morokuma, K. M. Nicholas, R. Periana, L. Que, J. Rostrup-Nielsen, W. M. H. Sachtler, L. D. Schmidt, A. Sen, G. A. Somorjai, P. C. Stair, B. Ray Stults, W. Tumas, *Chem. Rev.* **2001**, *101*, 953.
- [81] N. Dietl, M. Engeser, H. Schwarz, *Angew. Chem., Int. Ed.* **2009**, *48*, 4861.
- [82] R. Francke, R. D. Little, *Chem. Soc. Rev.* **2014**, *43*, 2492.
- [83] M. Yan, Y. Kawamata, P. S. Baran, *Chem. Rev.* **2017**, *117*, 13230.
- [84] S. Möhle, M. Zirbes, E. Rodrigo, T. Gieshoff, A. Wiebe, S. R. Waldvogel, *Angew. Chem., Int. Ed.* **2018**, *57*, 6018.
- [85] N. L. Weinberg, H. R. Weinberg, *Chem. Rev.* **1968**, *68*, 449.
- [86] K. J. Lee, J. L. Dempsey, *ACS Cent. Sci.* **2017**, *3*, 1137.
- [87] R. G. Bergman, *Nature* **2007**, *446*, 391.
- [88] A. N. Christensen, H. Kvande, P. G. Wahlbeck, E. Näsäkkälä, *Acta Chem. Scand.* **1977**, *31a*, 509.
- [89] S. Y. Tang, R. A. Bourne, R. L. Smith, M. Poliakoff, *Green Chem.* **2008**, *10*, 268.
- [90] S. L. Y. Tang, R. L. Smith, M. Poliakoff, *Green Chem.* **2005**, *7*, 761.
- [91] J. Jang, K. Shen, C. G. Morales-Guio, *Joule* **2019**, *3*, 2589.
- [92] L. Zhou, J. M. P. Martirez, J. Finzel, C. Zhang, D. F. Swearer, S. Tian, H. Robotajazi, M. Lou, L. Dong, L. Henderson, P. Christopher, E. A. Carter, P. Nordlander, N. J. Halas, *Nat. Energy* **2020**, *5*, 61.
- [93] H. Song, X. Meng, Z. Wang, H. Liu, J. Ye, *Joule* **2019**, *3*, 1606.
- [94] S. Sirajuddin, A. C. Rosenzweig, *Biochemistry* **2015**, *54*, 2283.
- [95] T. J. Lawton, A. C. Rosenzweig, *J. Am. Chem. Soc.* **2016**, *138*, 9327.
- [96] M. Stoukides, *J. Appl. Electrochem.* **1995**, *25*, 899.
- [97] S. Xie, S. Lin, Q. Zhang, Z. Tian, Y. Wang, *J. Energy Chem.* **2018**, *27*, 1629.
- [98] T. Otagawa, *J. Electrochem. Soc.* **1985**, *132*, 2951.
- [99] A. M. Couper, D. Pletcher, F. C. Walsh, *Chem. Rev.* **1990**, *90*, 837.
- [100] A. H. Bagherzadeh Mostaghimi, T. A. Al-Attas, M. G. Kibria, S. Siahrostami, *J. Mater. Chem. A* **2020**, *8*, 15575.
- [101] A. H. Taylor, S. B. Brummer, *J. Phys. Chem.* **1968**, *72*, 2856.
- [102] W. T. Grubb, C. J. Michalske, *Nature* **1964**, *201*, 287.
- [103] S. Y. Hsieh, *J. Electrochem. Soc.* **1977**, *124*, 1171.
- [104] L. W. Niedrach, *J. Electrochem. Soc.* **1964**, *111*, 1309.
- [105] K. W. Frese, *Langmuir* **1991**, *7*, 13.
- [106] J. Qiao, S. Tang, Y. Tian, S. Shuang, C. Dong, M. M. F. Choi, *Sens. Actuators B-Chem* **2009**, *138*, 402.
- [107] R. S. Rocha, L. M. Camargo, M. R. V. Lanza, R. Bertazzoli, *Electrocatalysis* **2010**, *1*, 224.
- [108] R. S. Rocha, R. M. Reis, M. R. V. Lanza, R. Bertazzoli, *Electrochim. Acta* **2013**, *87*, 606.
- [109] K. Ogura, K. Takamagari, *Nature* **1986**, *319*, 308.
- [110] K. Ogura, C. T. Migita, Y. Ito, *J. Electrochem. Soc.* **1990**, *137*, 500.
- [111] M. Ma, B. J. Jin, P. Li, M. S. Jung, J. Il Kim, Y. Cho, S. Kim, J. H. Moon, J. H. Park, *Adv. Sci.* **2017**, *4*, 1700379.
- [112] J. Nandena, E. H. Fontes, R. M. Piasentin, F. C. Fonseca, A. O. Neto, *J. Fuel Chem. Technol.* **2018**, *46*, 1137.

- [113] K. Otsuka, I. Yamanaka, *Catal. Today* **1998**, *41*, 311.
- [114] I. Yamanaka, S. Hasegawa, K. Otsuka, *Appl. Catal. A-Gen.* **2002**, *226*, 305.
- [115] B. Lee, T. Hibino, *J. Catal.* **2011**, *279*, 233.
- [116] M. Ma, C. Oh, J. Kim, J. H. Moon, J. H. Park, *Appl. Catal., B* **2019**, *259*, 118095.
- [117] Y. Song, Y. Zhao, G. Nan, W. Chen, Z. Guo, S. Li, Z. Tang, W. Wei, Y. Sun, *Appl. Catal. B-Environ.* **2020**, *270*, 118888.
- [118] Z. Guo, W. Chen, Y. Song, X. Dong, G. Li, W. Wei, Y. Sun, *Chin. J. Catal.* **2020**, *41*, 1067.
- [119] Y. Amenomiya, V. I. Birss, M. Goledzinowski, J. Galuszka, A. R. Sanger, *Catal. Rev.* **1990**, *32*, 163.
- [120] N. Spinner, W. E. Mustain, *ECS Trans.* **2013**, *53*, 1.
- [121] N. Spinner, W. E. Mustain, *Electrochim. Acta* **2011**, *56*, 5656.
- [122] M. Fleischmann, K. Korinek, D. Pletcher, *J. Electroanal. Chem. Interfacial Electrochem.* **1971**, *31*, 39.
- [123] T. J. Omasta, W. A. Rigdon, C. A. Lewis, R. J. Stanis, R. Liu, C. Q. Fan, W. E. Mustain, *ECS Trans.* **2015**, *66*, 129.
- [124] A. Tomita, J. Nakajima, T. Hibino, *Angew. Chem., Int. Ed.* **2008**, *47*, 1462.
- [125] M. Lersch, M. Tilset, *Chem. Rev.* **2005**, *105*, 2471.
- [126] A. E. Shilov, G. B. Shul'pin, *Chem. Rev.* **1997**, *97*, 2879.
- [127] C. I. Herrerías, X. Yao, Z. Li, C.-J. Li, *Chem. Rev.* **2007**, *107*, 2546.
- [128] S. F. Liu, F. Nusrat, *Mol. Catal.* **2019**, *463*, 16.
- [129] M. S. Freund, J. A. Labinger, N. S. Lewis, J. E. Bercaw, *J. Mol. Catal.* **1994**, *87*, L11.
- [130] R. S. Kim, Y. Surendranath, *ACS Cent. Sci.* **2019**, *5*, 1179.
- [131] A. Rauf, M. S. Arif Sher Shah, J. Y. Lee, C. H. Chung, J. W. Bae, P. J. Yoo, *RSC Adv.* **2017**, *7*, 30533.
- [132] A. Rauf, M. S. A. Sher Shah, G. H. Choi, U. Bin Humayoun, D. H. Yoon, J. W. Bae, J. Park, W. J. Kim, P. J. Yoo, *ACS Sustainable Chem. Eng.* **2015**, *3*, 2847.
- [133] M. S. A. Sher Shah, A. R. Park, K. Zhang, J. H. Park, P. J. Yoo, *ACS Appl. Mater. Interfaces* **2012**, *4*, 3893.
- [134] M. S. A. Sher Shah, K. Zhang, A. R. Park, K. S. Kim, N.-G. Park, J. H. Park, P. J. Yoo, *Nanoscale* **2013**, *5*, 5093.
- [135] X. Chen, X. Huang, Z. Yi, *Chem. - Eur. J.* **2014**, *20*, 17590.
- [136] X. Chen, Y. Li, X. Pan, D. Cortie, X. Huang, Z. Yi, *Nat. Commun.* **2016**, *7*, 12273.
- [137] J. Baltrusaitis, I. Jansen, J. D. Schuttlefield Christus, *Catal. Sci. Technol.* **2014**, *4*, 2397.
- [138] Z. Zakaria, S. K. Kamarudin, *Renew. Sustain. Energy Rev.* **2016**, *65*, 250.
- [139] S. L. Kaliaguine, B. N. Shelimov, V. B. Kazansky, *J. Catal.* **1978**, *55*, 384.
- [140] M. D. Ward, J. F. Brazdil, S. P. Mehandru, A. B. Anderson, *J. Phys. Chem.* **1987**, *91*, 6515.
- [141] K. R. Thampi, J. Kiwi, M. Grätzel, *Catal. Lett.* **1988**, *1*, 109.
- [142] M. Graetzel, K. R. Thampi, J. Kiwi, *J. Phys. Chem.* **1989**, *93*, 4128.
- [143] Z. Li, X. Pan, Z. Yi, *J. Mater. Chem. A* **2019**, *7*, 469.
- [144] C. E. Taylor, *Top. Catal.* **2005**, *32*, 179.
- [145] F. Sastre, V. Fornés, A. Corma, H. García, *J. Am. Chem. Soc.* **2011**, *133*, 17257.
- [146] M. Gondal, A. Hameed, A. Suwaiyan, *Appl. Catal. A-Gen.* **2003**, *243*, 165.
- [147] A. Hameed, I. M. I. Ismail, M. Aslam, M. A. Gondal, *Appl. Catal. A-Gen.* **2014**, *470*, 327.
- [148] K. Villa, S. Murcia-López, T. Andreu, J. R. Morante, *Appl. Catal. B-Environ.* **2015**, *163*, 150.
- [149] K. Villa, S. Murcia-López, J. R. Morante, T. Andreu, *Appl. Catal. B-Environ.* **2016**, *187*, 30.
- [150] M. Tahir, B. Tahir, N. S. Amin, *Mater. Res. Bull.* **2015**, *63*, 13.
- [151] N. Yazdanpour, S. Sharifnia, *Sol. Energy Mater. Sol. Cells* **2013**, *118*, 1.
- [152] M. Akbari, S. Sharifnia, *Mater. Lett.* **2017**, *194*, 110.
- [153] S. Wu, Y. Li, Q. Zhang, Z. Jiang, Y. Yang, J. Wu, X. Zhao, *Energy Environ. Sci.* **2019**, *8*, 1702472.
- [154] J. Yang, W. Xiao, X. Chi, X. Lu, S. Hu, Z. Wu, W. Tang, Z. Ren, S. Wang, X. Yu, L. Zhang, A. Rusydi, J. Ding, Y. Guo, P.-X. Gao, *Appl. Catal. B-Environ.* **2020**, *265*, 118469.
- [155] J. Yang, J. Hao, J. Wei, J. Dai, Y. Li, *Fuel* **2020**, *266*, 117104.
- [156] H. Song, X. Meng, S. Wang, W. Zhou, X. Wang, T. Kako, J. Ye, *J. Am. Chem. Soc.* **2019**, *141*, 20507.
- [157] S. Shoji, X. Peng, A. Yamaguchi, R. Watanabe, C. Fukuhara, Y. Cho, T. Yamamoto, S. Matsumura, M.-W. Yu, S. Ishii, T. Fujita, H. Abe, M. Miyauchi, *Nat. Catal.* **2020**, *3*, 148.
- [158] J. Xie, R. Jin, A. Li, Y. Bi, Q. Ruan, Y. Deng, Y. Zhang, S. Yao, G. Sankar, D. Ma, J. Tang, *Nat. Catal.* **2018**, *1*, 889.
- [159] K. Wada, H. Yamada, Y. Watanabe, T. A. Mitsudo, *J. Chem. Soc., Faraday Trans.* **1998**, *94*, 1771.
- [160] M. Anpo, I. Tanahashi, Y. Kubokawa, *J. Phys. Chem.* **1982**, *86*, 1.
- [161] V. Krishna, V. S. Kamble, P. Selvam, N. M. Gupta, *Catal. Lett.* **2004**, *98*, 113.
- [162] X. Chen, Y. Li, X. Pan, D. Cortie, X. Huang, Z. Yi, *Nat. Commun.* **2016**, *7*, 1.
- [163] Y. Hu, S. Higashimoto, S. Takahashi, Y. Nagai, M. Anpo, *Catal. Lett.* **2005**, *100*, 35.
- [164] R. P. Noceti, C. E. Taylor, J. R. D'Este, *Catal. Today* **1997**, *33*, 199.
- [165] G. Chen, G. I. N. Waterhouse, R. Shi, J. Zhao, Z. Li, L. Z. Wu, C. H. Tung, T. Zhang, *Angew. Chem., Int. Ed.* **2019**, *58*, 17528.
- [166] F. Sastre, V. Fornés, A. Corma, H. García, *Chem. - Eur. J.* **2012**, *18*, 1820.
- [167] M. A. Gondal, A. Hameed, Z. H. Yamani, A. Arfaj, *Chem. Phys. Lett.* **2004**, *392*, 372.
- [168] K. Villa, S. Murcia-López, T. Andreu, J. R. Morante, *Catal. Commun.* **2015**, *58*, 200.
- [169] B. Han, W. Wei, L. Chang, P. Cheng, Y. H. Hu, *ACS Catal.* **2016**, *6*, 494.
- [170] H. Liu, X. Meng, T. D. Dao, H. Zhang, P. Li, K. Chang, T. Wang, M. Li, T. Nagao, J. Ye, *Angew. Chem., Int. Ed.* **2015**, *54*, 11545.
- [171] H. Liu, T. D. Dao, L. Liu, X. Meng, T. Nagao, J. Ye, *Appl. Catal. B-Environ.* **2017**, *209*, 183.
- [172] Y. Zhao, W. Gao, S. Li, G. R. Williams, A. H. Mahadi, D. Ma, *Joule* **2019**, *3*, 920.
- [173] S. L. Miller, *Science* **1953**, *117*, 528.
- [174] K. Harada, S. W. Fox, *Nature* **1964**, *201*, 335.
- [175] C. A. Ponnamperna, M. Calvin, R. Mariner, R. M. Lemmon, *Proc. Natl. Acad. Sci. USA* **1963**, *49*, 737.
- [176] S. L. Miller, *J. Am. Chem. Soc.* **1955**, *77*, 2351.
- [177] S. Synthesis, A. Acids, *Science* **1970**, *168*, 470.
- [178] C. Sagan, B. N. Khare, *Science* **1971**, *173*, 417.
- [179] H. Reiche, A. J. Bard, *J. Am. Chem. Soc.* **1979**, *101*, 3127.
- [180] W. W. Dunn, Y. Aikawa, A. J. Bard, *J. Am. Chem. Soc.* **1981**, *103*, 6893.
- [181] K. Ogura, C. T. Migita, M. Fujita, *Ind. Eng. Chem. Res.* **1988**, *27*, 1387.
- [182] F. Che, J. T. Gray, S. Ha, N. Kruse, S. L. Scott, J. S. McEwen, *ACS Catal.* **2018**, *8*, 5153.
- [183] C.-H. Yeh, T. M. Le Pham, S. Nachimuthu, J.-C. Jiang, *ACS Catal.* **2019**, *9*, 8230.
- [184] Y. Sekine, M. Haraguchi, M. Matsukata, E. Kikuchi, *Catal. Today* **2011**, *171*, 116.
- [185] K. Oshima, T. Shinagawa, Y. Sekine, *J. Jpn. Pet. Inst.* **2013**, *56*, 11.
- [186] L. Wang, Y. Yi, C. Wu, H. Guo, X. Tu, *Angew. Chem., Int. Ed.* **2017**, *56*, 13679.
- [187] S. Jin, *ACS Energy Lett.* **2018**, *3*, 2610.
- [188] L. Zhang, L. Liardet, J. Luo, D. Ren, M. Grätzel, X. Hu, *Nat. Catal.* **2019**, *2*, 366.
- [189] J. Liu, Y. Zou, B. Jin, K. Zhang, J. H. Park, *ACS Energy Lett.* **2019**, *4*, 3018.
- [190] A. S. Alsuhaibani, S. Afzal, M. Challiwala, N. O. Elbashir, *Catal. Today* **2020**, *343*, 191.



**Md. Selim Arif Sher Shah** completed his Ph.D. in Chemistry on nanocomposite solid polymer electrolytes from Osmania University (dissertation work was carried out at Indian Institute of Chemical Technology (IICT)) Hyderabad, India. He is now a research professor in the Department of Chemical and Biomolecular Engineering at Yonsei University. Prior to this, he was a postdoctoral researcher at Sungkyunkwan University. He has been working on graphene-based nanostructured hybrid materials for photocatalysis, electrocatalysis, and lithium ion battery anode materials. His current research activities focus on fundamental understanding of catalysis and development of novel nanocatalysts for photochemical and electrochemical energy conversion applications.



**Jong Hyeok Park** is a professor in the department of chemical and biomolecular engineering at Yonsei University, Republic of Korea. He received his Ph.D. in Chemical Engineering from KAIST, Republic of Korea, in August 2004. Then, he joined the University of Texas at Austin, USA, as a postdoctoral researcher in 2004 (under Prof. Allen J. Bard). From March 2007 to February 2008, he worked at ETRI. His research focuses on solar-to Li & Na ion batteries, perovskite and organic solar cells, and solar-to-hydrogen conversion devices.